Title

Challenges for the theoretical description of the mechanism and kinetics of reactions catalyzed by zeolites

Authors

Van der Mynsbrugge, Jeroen
Bell, Alexis T

Publication Date

2021-12-01

DOI

10.1016/j.jcat.2021.08.048

Peer reviewed

Journal of Catalysis 404 (2021) 832–849

Contents lists available at ScienceDirect

Journal of Catalysis

journal homepage: www.elsevier.com/locate/jcat

Mini-review

Challenges for the theoretical description of the mechanism and kinetics of reactions catalyzed by zeolites

Jeroen Van der Mynsbrugge, Alexis T. Bell *

Department of Chemical and Biomolecular Engineering, University of California, Berkeley, CA 94720, United States

ARTICLE INFO

Article history:
Received 9 June 2021
Revised 7 August 2021
Accepted 26 August 2021
Available online 6 September 2021

ABSTRACT

Zeolites are widely used as catalysts for the processing of petroleum to produce transportation fuels, the synthesis of a wide variety of chemicals, and for the abatement of automotive emissions. These applications have stimulated an interest in describing the mechanism and kinetics for zeolite-catalyzed reactions using theoretical methods. This Mini-review summarizes the author's efforts towards this goal. It is shown that accurate predictions of adsorption and activation enthalpies and entropies requires that several criteria be met. The first is a correct description of the structure of the catalytically active center, as well as the portion of the zeolite framework immediately surrounding the active center and that located far from the active center. Second, the level of density functional theory (DFT) must be sufficiently high to account for the effects of dispersive interactions between the adsorbate, the active center, and the immediately surrounding zeolite atoms. Third, dispersive and coulombic interactions between the atoms in the vicinity of the active center and the balance of the zeolite framework must also be accounted for. It is shown that these conditions can be met using hybrid quantum mechanics/molecular mechanics (QM/MM) together with a high-level exchange-correlation functional and a large basis set. The success of our QM/MM approach is illustrated for reactions of light alkanes in H-MFI, as well as other protonated zeolites, and in Ga/H-MFI. We show that for low temperatures (<400 K), the QM/MM approach gives good predictions of molecular adsorption enthalpies and activation enthalpies for elementary reactions. This is also true for higher temperatures (>400 K) if the effects of configuration are considered using a correction obtained from configurationally biased Monte Carlo (CBMC) calculations. Calculations of the molecular adsorption entropy and the activation entropy for elementary reactions are more difficult to predict accurately. Application of the quasi-rigid rotor harmonic approximation overpredicts the loss of entropy of adsorption from the gas phase, particularly for zeolites containing large cavities and channels. CBMC corrections capture this deviation well for molecular adsorption and for early transition states resembling the adsorbed state but are inadequate for late transition states involving two loosely associated fragments.

1. Introduction

Zeolites are used to promote the conversion of petroleum to transportation fuels and the synthesis of a broad range of chemicals, as well as for the abatement of automotive exhaust emissions and account for nearly a fifth of all catalysts sold annually [1] The catalytically active sites in zeolites can take various forms - Brønsted acid protons, metal cations (isolated and in small clusters), and nanoclusters of metal or metal oxide. Because the pores and channels contained in the zeolite framework fall in the range of 0.1–1.0 nm, the activity and selectivity of the active sites are influenced not only by the properties of the site but also by their confinement within volumes of molecular dimensions. For these reasons, both the activity and selectivity of active sites are strongly influenced by the architecture of the zeolite pores and channels. Consequently, it is necessary to know not only how reactants and products interact with the active site but also with the portions of the zeolite confining the active site. The atoms and cations comprising the balance of the zeolite framework also influence the performance of the active site through van der Waals and Coulombic interactions.

* Corresponding author.
E-mail address: alexbell@berkelye.edu (A.T. Bell).

https://doi.org/10.1016/j.jcat.2021.08.048
0021-9517/

The kinetics by which reactants are converted to products are dictated by the Gibbs free energy landscape on which the reaction occurs. This landscape is defined by the positions of the atoms in the active center and all atoms comprising the reactants, intermediates, and products. The lowest free energy pathway from reactants to products is defined by the elementary steps involved in transforming reactants to products, referred to collectively as the reaction mechanism. If a plausible mechanism for a reaction can be postulated on the basis of known chemistry or can be deduced from independent experimental evidence of adsorbed reactants, intermediates, and products, then theoretical methods can be used to estimate the free energy landscape for that mechanism. Since the free energy involves enthalpic and entropic contributions ($\Delta G = \Delta H - T\Delta S$) both terms must be determined accurately if the free energy landscape is to be useful for determining the extent to which one, or a subset, of the elementary reactions controls the overall kinetics.

In this Mini-review, the author gives his perspective on the current state of the art for determining the enthalpic and entropic contributions to the free energy of reactions catalyzed by active centers contained in zeolites. It will be shown that advances in density functional theory (DFT) enable calculation of adsorption and activation enthalpies with near chemical accuracy, but accurate calculation of entropies of adsorption and activation remains an ongoing challenge. Thoughts on how to make progress on the latter subject will also be presented.

2. Reaction kinetics

The overall rates of reactant consumption and product formation can be described using a microkinetic model based on either an assumed mechanism or one deduced from independent studies of the reaction network [2]. The net rate of formation or consumption of any observable species (i.e., reactant and product) is given by the difference in the rates of formation and consumption of that species by all relevant elementary reactions. Any intermediates formed along the reaction pathway are assumed to rapidly attain a quasi-steady state for which the net rate of formation and consumption of the intermediate are nearly equal. In its simplest form, the rate of each elementary reaction is assumed to be given by the product of the rate coefficient for that step, k_{ij}, where i designates the species i and j designates elementary reaction j, and the fractional site occupancy θ_i (where i = 1 to I) or the product $\theta_i C_l$, where C_l is the local concentration of reactant l in the zeolite pore space near the active site. Using this nomenclature, the rate of an individual elementary step, r_{ij}, can be expressed as

$$r_{ij} = k_{ij}\theta_i \text{ or } r_{ij} = k_{ij}\theta_i C_l \tag{1}$$

and the overall rate of formation of species i, R_i, is given by

$$R_i = \sum_{j=1}^{J} \nu_{ij} r_{ij} \tag{2}$$

where ν_{ij} is the stoichiometric coefficient or species i in reaction j (positive for the formation of species i and negative for the consumption of species i) and the summation is over all elementary reactions that either produce or consume species j (j = *1 to J*). It should be noted that there are two important assumptions inherent in Eq. (1). The first is that k_{ij} is independent of the site occupancy of any species and the second is that the coverage of all adsorbed species is uniform throughout the zeolite (i.e., intrazeolite mass transfer is rapid). The first assumption is valid if there is no direct communication between the sites, i.e., that the sites are well isolated, as would be the case in zeolites with a high Si/Al ratio. However, for large reactant molecules and lower values of the Si/Al ratio, interference between adsorbates can affect the rate coefficient for an elementary step occurring at an otherwise isolated site [3]. The second assumption is also valid for isolated site catalysts provided the rate of mass transport between sites is faster than the rate of reaction at the site. Since the number of active sites is finite, the sum of all values of θ_i is equal to one, as given by Eq. (3).

$$\sum_{i=1}^{I} \theta_i = 1 \tag{3}$$

In general, the set of equations describing the kinetics are nonlinear because of the product term in surface coverage and species concentrations appearing in Eq. (1). For such systems, the model must be solved numerically to determine the rates of reactant consumption and product formation for a given set of reaction conditions; however, to do so requires knowledge of or estimates for all rate coefficients. On the other hand, if each of the elementary processes is unimolecular (or pseudo unimolecular) and the concentration of un-adsorbed species is uniform throughout the zeolite crystal (i.e., low reactant conversion), then the overall microkinetic model can be solved using matrix techniques without needing to know the values of the rate coefficients a priori. Further simplifications can be achieved if one or more elementary step can be taken to be rate-determining (see below) and subsequent elementary steps can be assumed to be kinetically irrelevant. Further simplification can be made if one or more of the elementary steps can be assumed to be at quasi-equilibrium. Under these circumstances, it is often possible to obtain an overall rate expression in closed form.

3. The role of theory in elucidating reaction pathways and reaction dynamics

During the past 30 years, theoretical methods have come to play an increasingly important role in understanding the mechanism by which catalyzed reactions occur and the dynamics of the elementary steps involved in the mechanism [4,5]. This impact of theory is a consequence of advances in efficient algorithms for calculating the electronic structure of ground and transition-state structures of adsorbed species and their energies and entropies, in addition to advances in computer speed and architecture. Additional reductions in computational burden have come from the development of hybrid methods for representing the extended structure of the catalyst beyond the active site. These advances have enabled meaningful application of theoretical methods for analyzing reaction pathways and estimating rate parameters for elementary reactions occurring over heterogeneous catalysts. In the balance of this section, we will examine the importance of basing theoretical calculations on a physically meaningful representation of the catalytically active sites and conducting calculations at the proper level of theory.

3.1. Structural models of catalytically active sites

Determining the structure of a catalytically active center and its interactions with adsorbed species requires a model of the active center and the surrounding environment. While chemistry occurs at the active center, the surrounding part of the zeolite influences its electronic properties and can interact with adsorbed species through dispersive and coulombic interactions. Two types of models are used most often to represent the catalyst – periodic models and cluster models [4-6]. Periodic models use a unit cell that can be repeated periodically to represent an unperturbed lattice (metal, metal oxide, zeolite, etc.), whereas cluster models use a finite fragment, or cluster, cut from the lattice of the catalyst. While a periodic model can naturally reproduce the full lattice of the host material, a cluster must be capped by H atoms or OH groups to replace the broken bonds at the edges of the fragment. These terminating atoms are typically fixed in space to prevent unphysical deviations from the crystallographic structure of the extended solid. Each type of model has its advantages and disadvantages. Cluster models must include a very large number of atoms to capture the complete effect of the extended solid on the energy of the adsorbed species, leading to high computational costs. Periodic models naturally describe the extended solid but may require large unit cells. The unit cell of the ubiquitous MFI zeolite contains 288 atoms. While some zeolites (e.g. CHA) have smaller unit cells, in these cases it is often necessary to utilize super cells to avoid artefacts due to spurious interactions between periodic images [6].

To mitigate the computational cost of large cluster models or large unit cells, multi-layer hybrid schemes have been employed by several authors [7-14]. In a divide-and-conquer approach, only a small cluster of atoms encompassing the active center of the catalyst and the adsorbates is treated quantum mechanically at a high level of theory. This small cluster is embedded within a larger model described using a less expensive level of theory such as a lower-level QM method or classical molecular mechanics (MM). A detailed discussion of the pros and cons of different hybrid schemes is beyond the scope of this paper and has been presented in a recent review [15]. In our studies, a QM/MM scheme is employed in which a small QM cluster is embedded within a much larger cluster in which all atoms remain at their crystallographic positions. The atoms of larger host cluster and their electrostatic and dispersive interactions with the atoms in the small cluster are described using analytical van der Waals and coulombic potentials. A typical cluster model used in our studies is shown in Fig. 1 [16].

3.2. Quantum mechanics

The theoretical framework for describing the structure and energetics of adsorbed species and transition states is quantum mechanics. Because the systems of interest for heterogeneous catalysis typically involve 10 s to 100 s atoms or more, solving the Schrodinger equation using traditional wave function methods is not practical. The most effective approach for studies in catalysis is Kohn-Sham density functional theory (DFT) [17], which represents the density of the interacting electrons by a single configuration of one-electron orbitals corresponding to a fictitious system of non-interacting electrons. The accuracy of DFT calculations depends on the quality of the functional used to approximate the non-classical exchange and electron-electron correlation and on the completeness of the atomic orbital basis set. Progress has been made in improving the quality of the exchange-correlation functional to minimize the error between the calculated and experimentally observed energies (see Ref. [15] for a discussion of this subject). While local generalized gradient approximation (GGA) functionals (e.g. PBE, B97) are still used because of their computational efficiency, it is now recognized that neglect of dispersion effects can be significant for many systems. Consequently, the use of dispersion-corrected GGAs, such as B97-D3 and PBE-D3, has become standard since the dispersion correction adds virtually zero additional computational cost. Hybrid GGA functionals that include exact HF exchange (e.g. B3LYP, M06, M06-2X) provide significantly more accuracy for chemical applications through a reduced self-interaction error, which causes artificial stabilization of transition states and leading to an underestimation of activation energies. In a recent benchmarking study, the range-separated and dispersion corrected hybrid GGA ωB97X-D used extensively in the author's work has been shown to provide good all-round performance for the description of thermochemistry, kinetics, and non-covalent interactions. Out of the 200 density functionals evaluated by Mardirossian and Head-Gordon, the very recently developed meta hybrid GGA ωB97M-V emerged as the best performer for thermochemistry, barrier heights, noncovalent interactions, and isomerization energies, showing great promise for future applications

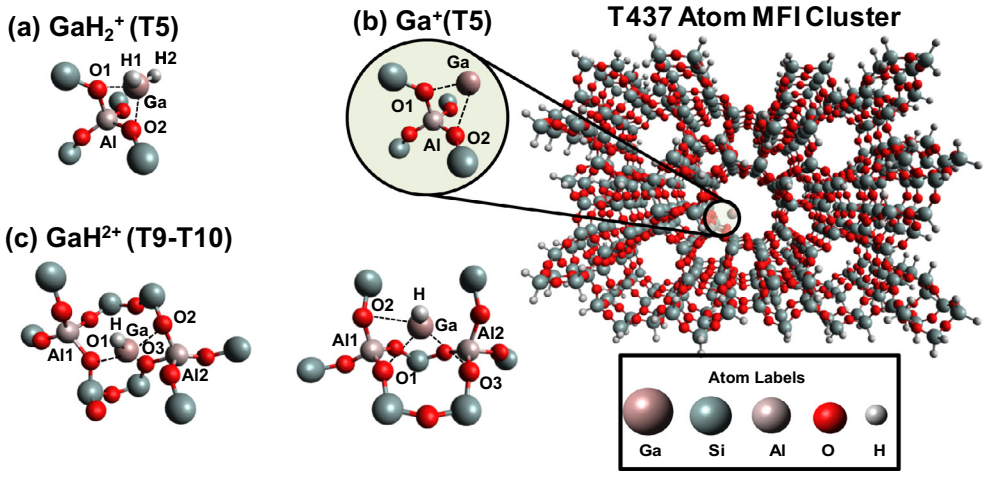

Fig. 1. View along [010] axis of T437 atom MFI structure used to model gallium-exchanged sites in Ga/HMFI: (a) $[GaH_2]^+$ (b) Ga^+ (c) $[GaH]^{2+}$. Two different Al-pair configurations (A and B) have been chosen based on different Al-Al distances. Configuration A is modeled using a T10 cluster while Configuration B is modeled using a T9 cluster. Reproduced by permission from Ref. [16].

[18]. While hybrid functionals such as B3LYP, HSE and PBE0 are nowadays available in several periodic codes, their usage is still not common in the field of zeolite catalysis. Because of the significantly higher computational expense, routine usage of (meta) hybrid GGAs is not yet feasible for calculations zeolite systems that require large unit cells or super cells.

It should be noted that the performance of all functionals is optimized for the complete atomic orbital basis set. While extrapolation to the complete basis set limit makes sense for small molecules, it is impractical due to computational cost associated with the description of large, complex systems typically encountered in heterogeneous catalysis. Therefore, polarized basis sets of triple zeta quality are typically used [15]. Ideally, computational results would be compared against specific and accurate experimental benchmarking data (e.g., heats of adsorption, turnover frequencies of individual elementary reactions). Unfortunately, such data is often unavailable or even unobtainable for zeolite systems. Nevertheless, the choice of models and methods can and should be evaluated from a computational perspective. The most rigorous validation then involves ensuring convergence of the results in terms of the size of the zeolite model, the size of the QM region, the DFT functional and the basis set (see, e.g., Ref. [30]). Often chemical intuition can be used for a more pragmatic approach. A suitable QM region should be large enough to represent all specific interactions (other than long-range electrostatics and dispersive interactions) between reactants or transition states and the active site. Careful inspection of the optimized geometries with this in mind can provide an *a posteriori* validation of the choice of QM region. The reliability of the chosen DFT functional for describing the system and properties of interest can be assessed by consulting benchmarking studies such as Ref. [18].

3.3. Determination of reactant and transition states

As noted earlier, chemical reactions occur on a complex, multidimensional free energy surface. Since quantum calculations are done without consideration of atomic and molecular motion they are de facto carried out at 0 K. In this case, the free energy surface becomes equivalent to the potential energy surface (PES). The minima on this surface represent stable adsorbed species (reactant, intermediates, and products), whereas the saddle points represent transition states between stable states [4]. To assess the energy and enthalpy profile for a reaction network, it is necessary to identify the minima and the transition states connecting minima. For large systems involving many atoms in the adsorbed and transition states, determination of minima and saddle points on the PES requires algorithms that are both efficient and accurate. Furthermore, the most efficient transition structure (saddle point) optimization methods require an initial guess that is close enough to the final structure has a second derivative matrix (i.e., the Hessian) with the correct structure – one negative eigenvalue, and the remainder positive. This means that skill and experience are required to successfully execute transition structure searches. Novel methods aimed at lowering the amount of chemical intuition and effort required on the part of the user are an expanding area of research. In a recent review paper, Zimmerman and coworkers discuss several existing semi-automated approaches as well as potential future advances for finding transition states and exploring reaction networks [19]. Below, we highlight an approach for handling this problem developed by the authors.

Our approach to finding transition states builds on the literature of double-ended methods developed to either identify a transition state between two minima on the PES or to find an approximation to the transition state that can then be further refined [20] Such double-ended algorithms typically fall into two general categories: interpolating algorithms and path optimization algorithms. The interpolating algorithms such as Linear and Quadratic Synchronous Transit (LQST) attempt to find the transition state by deducing an approximate reaction pathway in a single pass, and then using a surface-walking algorithm to refine some midpoint of this pathway to the exact transition state. While these methods are simple and computationally inexpensive, they offer no recourse when they fail to locate a transition state. The reaction path optimization algorithms, such as the Nudged Elastic Band (NEB) method, String Method (SM), and Growing String Method (GSM) describe the reaction pathway as a series of molecular images (the "string"), and optimize the string iteratively until it rests along the reaction path. Once the reaction path is located, it is easy to identify the maximum energy node and use surface walking techniques to isolate the exact saddle point. Unfortunately, all interpolating methods require a large number of QM calculations for the string to obtain a reasonable estimate of the reaction path and transition state. Of particular note is that a large number of QM calculations are required for nodes on the outer portions of the string that are close to the reactant and product structures and far from the desired transition state. To overcome this limitation, we have developed the Freezing String Method (FSM), which minimize the number of QM calculations needed to obtain meaningful approximations to TS structures [20], This is achieved by freezing newly grown nodes after a fixed number of iterations. Consequently, expensive QM calculations are not wasted on settling the string of nodes into the reaction path where they do not describe the transition state anyway. The FSM can locate transition state structures with minimal user input and computational cost that is 50% or less than that required for the GSM.

3.4. Entropies of reaction and activation

Until relatively recently, theoretical analyses of reactions occurring on heterogeneous catalysts in zeolites have focused on accurate determinations of the enthalpy of reaction and the enthalpy of activation (the enthalpy difference between the transition state and the reactant state), both of which can be determined from DFT calculations. However, as already noted, the progress of any reaction is dictated by changes in the Gibbs free energy, rather than by enthalpy changes alone. The difference between the change in the Gibbs free energy and the change in the enthalpy is given by $-T\Delta S$, where ΔS is the change in entropy between the final and the initial state (product and reactant states or transition and reactant states). For reactions involving large reactants or two reactants, particularly for reactions occurring at high temperature, the magnitude of $-T\Delta S$ can become comparable to that of the enthalpy change, ΔH, and hence this contribution to the change in Gibbs free energy of activation cannot be neglected.

The entropies of reaction and activation are related to the ratios of the partition functions, Q, for the final and initial state:

$$\Delta S = R \ln \left(Q^{P} / Q^{R} \right) \tag{4}$$

or

$$\Delta S^{\ddagger} = R \ln \left(Q^{\ddagger} / Q^{R} \right) \tag{5}$$

The superscripts R, P, and ‡ refer to the reactant, product, and transition states, respectively. Each of the partition functions appearing in Eqs. (4) and (5) can be represented as

$$Q = Q_{trans} Q_{rot} Q_{vib} Q_{elec} \tag{6}$$

The partition function for each state contains contribution from global translation and rotation of the reactant (product), catalyst, or adsorbate-catalyst relative to a fixed set of Cartesian coordinates and a contribution due to internal vibrations of the reactant (product), catalyst, or adsorbate-catalyst. For gaseous reactants and products, global translations and rotations are treated using relations derived from statistical mechanics, whereas the catalyst and adsorbate-catalyst adduct are usually treated as being immovable and irrotational. The vibrational contribution to the overall partition function has traditionally been treated in the harmonic approximation (HO); however, recent research has shown that this approximation is inaccurate for both gas phase species and adsorbed species in cases where weak, anharmonic vibrations occur [21]. Accurate methods for treating the vibrational energy levels for small systems include the utilizing complete quartic force fields, and vibrational self-consistent field theory (VSCF), perturbation theory (VPT), configuration interaction (VCI), and coupled cluster theory (VCC), which correct the HO oscillator reference for higher than quadratic terms (see Ref. [22] and references cited therein). These methods, particularly the higher accuracy variants, have been quite successful for small systems, but, with the possible exception of the lower accuracy VSCF and PVT2, are not generally viable for larger molecules because of the computational cost.

Significant efforts have also been made to improve the accuracy of the calculated thermodynamic quantities for anharmonic systems. Path integral Monte Carlo (PIMC) and path integral molecular dynamics (PIMD) provide attractive fully numerical schemes to accurately calculate quantum mechanical partition functions with anharmonicity and mode-mode coupling effects considered [23,24]. However, due to high computational costs, applications of path integral methods are usually restricted to small systems. On the other hand, methods that represent the full-dimensional PES with tractable functions are more computationally feasible for medium or large size systems though mode-mode coupling effects must inevitably be neglected, at least to some extent. Piccini and Sauer have reported a computational protocol that uses normal mode coordinates to obtain optimized geometries and harmonic frequencies [21]. By using a fourth-order polynomial to approximate the anharmonic PES of the low-frequency modes, these authors were able predict adsorption free energies of small alkanes in H-CHA within chemical accuracy. While using low-order polynomials is computationally advantageous, it is challenging for nonexperts to gauge how discrepancies between the model and the real PES affect the accuracy of computed thermodynamic properties. A computational protocol for solving for the energy levels of PESs represented by cubic splines has been recently reported, which can accurately represent the PES of a mode, no matter whether it is a nearly harmonic bond stretch, or a highly anharmonic torsion [22]. The goal is to approach the limit of accuracy that is possible within the uncoupled mode (UM) approximation, in which case remaining errors are due to mode coupling. To generalize the methodology to larger molecules where internal rotations are important effects, another scheme was developed in which sampling of vibrations and internal rotations (UM-VT) are carried out separately. The UM-VT approximation significantly outperforms the UM-N and the HO approximations in calculations of partition functions and entropies. In enthalpy calculations, these three models performed almost equally well, but a slightly smaller error is obtained for UM-VT. The advantage of UM-VT approximation is that it allows a treatment of anharmonicity with computational costs that are comparable to those for the HO model.

4. Identification of rate-determining intermediates and rate-determining transition states from an analysis of the free energy landscape

The first-principles-based energetic-span model provides a useful conceptual tool for identifying the rate-limiting processes which control the kinetics of a catalytic cycle containing multiple elementary steps [25-28]. According to this model, the turnover frequency for a catalyzed reaction is governed by the transition state and intermediate which maximize the energetic span for a given catalytic cycle. This energetic span is determined by examining the free energy surface for the highest summit, the rate-determining transitions state (RDTS) and the lowest trough, the rate-determining intermediate (RDI), which then provides an estimate of the apparent free energy of activation ($\Delta G^{\ddagger}$) which must be overcome to complete a given catalytic cycle. However, the highest summit on the free energy profile may not always correspond to the TS which determines the turnover frequency (TOF). To determine the RDTS, what must first be computed is the energy difference between each intermediate I and transition state TS, where depending on whether the lowest lying resting state (RDI) occurs before or after TS, the energetic span for the catalytic cycle can be calculated via Eq. (7).

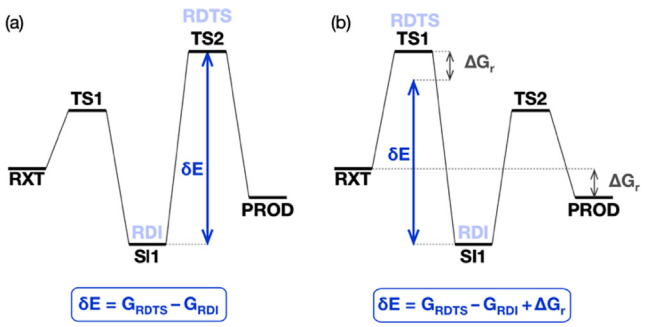

Fig. 2. Example illustrating the computation of free energy spans on a free energy landscape for (a) the case when the RDTS follows the RDI and (b) the case when the RDTS precedes the RDI. G_{RDTS} and G_{RDI} are the free energies of the turnover rate determining transition state and turnover rate determining resting states, respectively. ΔG_r is the total reaction free energy.

$$TOF = \frac{kT}{h}\frac{e^{-\frac{\Delta G_r}{RT}} - 1}{\sum_{i,j} e^{-\frac{TS_i - SI_j - \delta G_{ij}}{RT}}} \tag{7}$$

$$\delta G_{ij} = \Delta G_r \text{ if } i > j$$

$$= 0 \text{ if } i \leq j$$

Where ΔG_r is the total reaction free energy and TS_i and SI_j are the free energies of the i^{th} transition state and j^{th} adsorbed intermediate in the cycle, respectively. The denominator contains the summation of all the exponentials of Gibbs energy differences between all the combinations of intermediates (SI_j) and transition states (TS_i). The energetic span approximation reduces to the expression illustrated in Eq. (8) when one term dominates in the denominator of Eq. (7):

$$TOF = \frac{kT}{h} e^{-\frac{\delta E}{RT}} \tag{8}$$

$$\delta E = G_{RDTS} - G_{RDI} \text{ if } i > j$$

$$= G_{RDTS} - G_{RDI} + \Delta G_r \text{ if } i \leq j$$

Where δE is the free energy span and G_{RDTS} and G_{RDI} are the free energies of the turnover rate determining transition state and turnover rate determining resting states. δE can be estimated from the free energy surface of the catalytic cycle, as illustrated in Fig. 2.

It should be recognized that Eq. (8) only applies for reaction systems for which branching does not occurs due to competing pathways to a single product or to different products. Cases where branching occurs can also be handled via the methods described in Refs. [25-28] for systems involving isolated reaction centers where all the centers are assumed to be identical, as is the case for reaction occurring in zeolites or supported metal atoms or cations in general. For such systems, it is still possible to write an expression for the TOF using matrix techniques, but the result is much more complex than represented by Eq. (8). The critical components of the final expression for the TOF, however, continue to be the rate coefficients for the forward and reverse steps of each elementary step in the proposed reaction mechanism. Since each rate coefficient can be expressed as $k_i = kT/h \exp(-\Delta G_i/kT)$, the challenge is to determine ΔG_i accurately using the methods of quantum mechanics and statistical mechanics.

5. Catalysis by zeolites

In this section, we will present several examples taken from the author's work to illustrate the accuracy with which the QM/MM approach can be used to predict the enthalpies of reactant adsorption and the activation energies for elementary reactions involving hydrocarbons. After that, we will examine more closely the effects of confinement on these parameters, as well as the entropies of adsorption and activation.

5.1. Simulation of adsorption in zeolites

Reactant adsorption is the first step in all zeolite catalyzed reactions. Investigations by several groups have demonstrated that long-range dispersive interactions must be considered together with local interactions to achieve an accurate representation of the thermodynamics of adsorption. While dispersion-corrected DFT calculations carried out with large basis sets are capable of achieving good accuracy, as noted above, the computational costs for cluster calculations are very high because very large clusters are required (involving more than 150 tetrahedral (T) atoms) to fully capture the effects for dispersive interactions with the extended zeolite framework [30,31]. We have recently shown that the computational burden for such calculations can be reduced considerably using a QM/MM model consisting of a

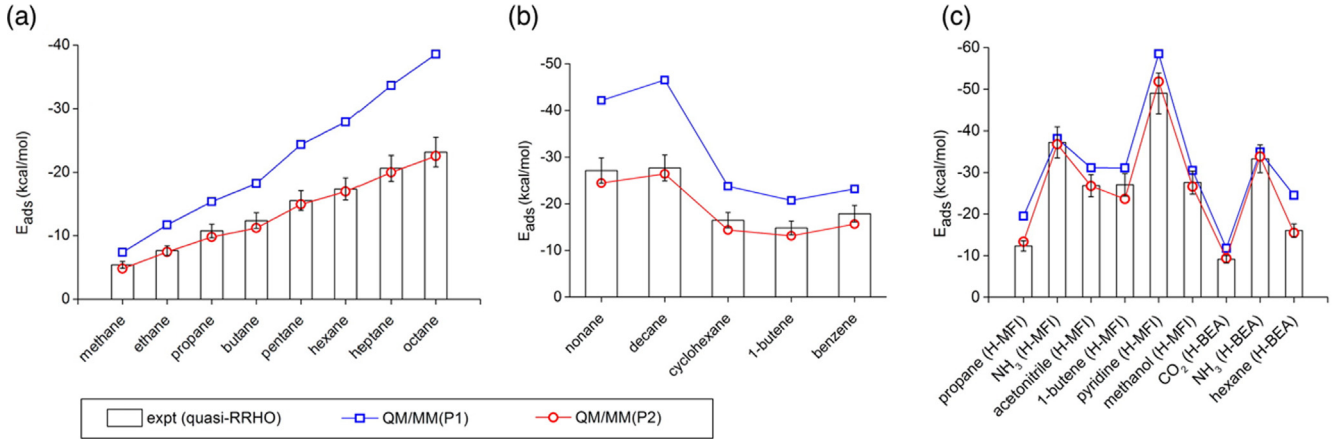

Fig. 3. Improved performance of P2 parameters for (a) training set, (b) and (c) test sets illustrating transferability to other adsorbates and zeolites. The predicted adsorption energies in (a) and (b) are calculated for guest molecules in siliceous MFI. Reproduced by permission from Ref. [31].

Table 1
Charge and Lennard-Jones Parameters for O and Si used for QM/MM simulations of hydrocarbon adsorption in MFI and Na-X (32, 33, 36).

Parameter set	$Q_{Si/Al}$	Q_O	Q_{Na}	$\varepsilon_{Si/Al}$ (kcal/mol)	R_{Si} (Å)	ε_O (kcal/mol)	R_O (Å)	ε_{Na} (kcal/mol)	R_{Na} (Å)
P1	0.7	−0.35	–	0.200	2.2	0.075	1.77	–	–
P2	0.7	−0.35	–	0.047	2.2	0.018	1.77	–	–
P2-Na	0.7	−0.58	1.0	0.047	2.2	0.018	1.77	0.0469	1.41
P3-Na	0.2	−0.35	0.0	0.047	2.2	0.018	1,77	0.0469	1.41

Table 2
Comparison of enthalpies of adsorption for C_1-C_7 alkanes in zeolite Na-X determined from QM/MM simulations and measured experimentally. The charge and Lennard-Jones parameters for O, Si/Al, and Na, parameter sets P2-Na and P3-Na used for the QM/MM calculations are given in Table 1.

	P3-Na	P2-Na	Expt. 1 [34]	Expt. 2 [35]	Expt. 3 [36]	Average Expt.
CH_4	−4.9	−7.8	−4.6	–	–	−4.6
C_2H_6	−6.3	−10.4	−6.5	–	–	−6.5
C_3H_8	−7.6	−15.2	–	−7.4	−6.8	−7.1
C_4H_{10}	−9.4	−17.2	–	–	−8.6	−8.6
C_5H_{12}	−11.5	−20.2	–	–	−10.5	−10.5
C_6H_{14}	−12.5	-23.5	–	–	−12.1	−12.1
C_7H_{16}	−14.1	−26.5	–	–	−14.7	−14.7
$\Delta H/CH_2$	−1.57	−3.12	−1.86	–	−1.94	−1.60
RMSD	0.63	7.73	–	–	–	–

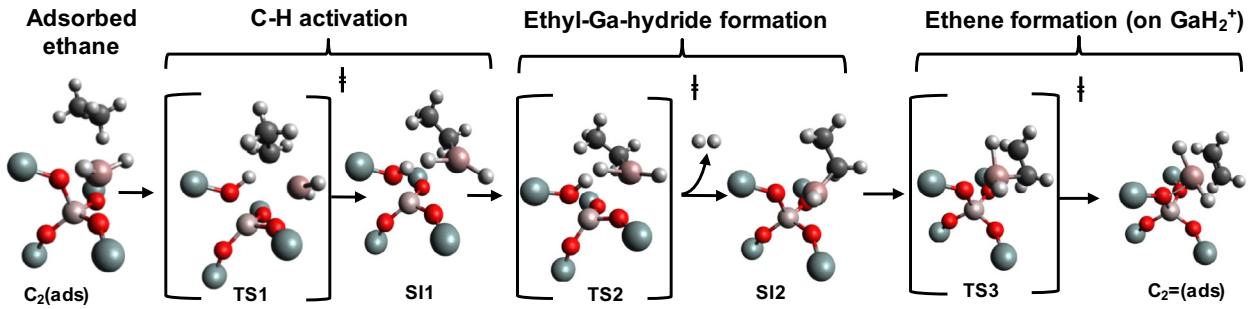

Fig. 4. Ethane dehydrogenation via Stepwise Alkyl Mechanism on GaH_2^+. Only the QM region from the QM/MM model has been displayed here to illustrate the elementary steps in this mechanism. Adapted from Ref. [15].

Table 3
A comparison of barrier height predictions using long-range corrected QM/MM versus prior finite QM cluster predictions in the literature. Electronic energy barriers ($\Delta E^{\ddagger}$) are calculated at 0 K for the dehydrogenation of light alkanes (C_2, C_3, nC_4 and iC_4) via the stepwise alkyl mechanism on $[GaH_2]^+$. The level of theory used to calculate the barriers are at ωB97X-D/6-31G(d,p) //ωB97X-D/6-311++G(3df,3pd). Reproduced by permission from Ref. [15].

Model Details	**Pereira et al.**[38]	**Pidko et al.**[39]	**Pereira et al.**[38]	**QM/MM**
Cluster Size	T5	T8	T22	T5(QM)/T435(MM)
DFT Functional	B3LYP	B3LYP	B3LYP	ωB97X-D
Basis Set	LACVP(d,p)	6-31G(d,p)	LACVP(d,p)	6–311++G(3df,3pd)
$\Delta E^{\ddagger}_{C2}$ **(kcal/mol)**	65	61.7	54.0	40.1
$\Delta E^{\ddagger}_{C3}$ **(kcal/mol)**	64.5	–	48.0	32.3
$\Delta E^{\ddagger}_{nC4}$**(kcal/mol)**	57.5	–	50.5	32.3
$\Delta E^{\ddagger}_{iC4}$ **(kcal/mol)**	59.5	–	49.6	32.9

5 T atom cluster treated quantum mechanically and a 200–400 T atom cluster treated by molecular mechanics. QM energy calculations were done at the ωB97X-D/6-311++G(3df,3pd) level of theory [29-31]. Standard CHARMM parameters were used for all atoms of the adsorbate but parameters for the atoms of the zeolite cluster were adjusted to obtain agreement between calculated and experimentally measured energies of adsorption for C_1 to C_8 *n*-alkanes in MFI. Zero-point corrections to the calculated energies were carried using the quasi-RRHO approximation [32].

Fig. 3a and 3b show that excellent agreement between the measured and calculated energies of adsorption for C_1 to C_8 *n*-alkanes in MFI can be obtained from QM/MM calculation in which the MM parameters were optimized to achieve the observed agreement. This corresponds to parameter set P2 given in Table 1. The same set of MM parameters was used to calculate the energies of adsorption for other adsorbates. Fig. 3c demonstrates excellent agreement between the measured and calculated energies of adsorption for both polar and non-polar adsorbates, and the same level of agreement is achieved when the adsorbent is changed from MFI to BEA. It is notable that while parameter set P1 gives excellent agreement of the adsorption energy determined from the QM/MM model with that determined from a 36T

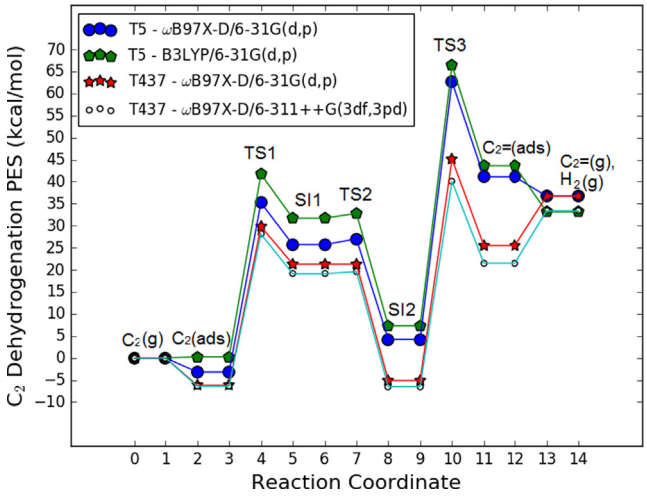

Fig. 5. Comparison of 0 K potential energy landscapes generated using QM/MM (T5:T437) and finite QM (T5) clusters. The potential energies represented here are the zero-point corrected electronic energies for the dehydrogenation of ethane via the stepwise alkyl mechanism on $[GaH_2]^+$. SI stands for Surface Intermediate. Larger clusters significantly stabilize TS3, with smaller effects associated with the choice of basis set and functional. Reproduced by permission from Ref. [15].

atom QM calculation [31] the agreement with experimental measurement deviates. This illustrates the need to capture the effects of long-range interactions using a sufficiently large representation of the zeolite lattice.

The same MM parameter set used to calculate the adsorption energies for MFI and BEA has also been used to calculate the enthalpies of adsorption for C_1 to C_7 *n*-alkanes in Na-X (with unit cell composition $Na_{96}Al_{96}Si_{96}O_{384}$) [33]. In this case, the QM region contains one Na cation 5T atoms and all adsorbate atoms. Table 2 shows that the enthalpy of adsorption is sensitive to the charge chosen for the Na^+ cations in the MM portion of the cluster. While the physically meaningful value for the charge is + 1, use of this value led to a ten-fold higher root-mean square deviation (RMSD) between the calculated and the experimentally observed enthalpy of adsorption and to a nearly two-fold higher value in the slope of the calculated change in enthalpy per CH_2 group relative to experiment. On the other hand, very good agreement between calculations and experiment was achieved by taking the charge of MM Na cations to be zero. Careful analysis reveals that use of a positive charge on the MM Na cations results in excessive polarization of atoms in the QM cluster, and that this problem becomes more severe with increasing number of C atoms in the adsorbate. This illustration points out a weakness of the QM/MM model for systems in which highly polarizing cations are located near the boundary of the QM and MM regions.

Further insights into the importance of long-range interactions and the level of theory on the quality of the computed enthalpy and entropy profiles were obtained in the course of our studies of alkane dehydrogenation over Ga/H-MFI. These insights were obtained from an analysis of ethane dehydrogenation on $[GaH_2]^+$. As discussed in more detail below, this reaction occurs via the stepwise alkyl mechanism illustrated in Fig. 4 [15,37]. Since earlier studies had predicted barriers using the zero-point corrected potential energy surface (PES) rather than the free energy surface, we evaluated these barriers using our QM/MM approach and report them in Table 3.

The activation barrier heights predicted by QM/MM and shown in Table 3 are significantly lower than those reported previously because of the added long-range corrections in the QM/MM calculations. The individual effects of functional, basis set, and cluster size, on these barrier heights were also explored. The PES for this process is shown by the hollow circles and light blue-line plotted in Fig. 5 [15] Also plotted in this figure are potential energy landscapes generated by varying the cluster size (T437 versus full QM T5), basis set (6-311++G(3df,3pd) versus 6-31G(d,p)) and functional (ωB97X-D versus B3LYP). The contribution of individual effects to the predicted barrier height for the TS3 bottleneck is shown in Table 4.

The results presented in Table 4 reveal that a barrier change of −5.0 kcal/mol for TS3 can be attributed to basis set incompleteness while a barrier change of −6.5 kcal/mol can be attributed to a change of functional. This latter difference occurs due to the added dispersion and range separation effects included in ωB97X-D, but which are neglected by B3LYP. A change in cluster size has the most significant impact, −17.6 kcal/mol, on the stabilization of TS3 due to long-range dispersion and electrostatics. We also find that the dipole moment of TS3 (relative to SI2) increases from 2.2 Debye to 3.5 Debye when going from a T5 to T437 cluster, suggesting that the stronger polarization of TS3 (when compared with SI2) is a consequence of the inclusion of the electrostatic field of the framework in the QM/MM model. Taken together, these results enable us to rationalize the substantial decrease in the predicted barrier for ethane dehydrogenation determined using QM/MM. This conclusion is also generally valid for other reactions systems, thereby pointing out the importance of considering long-range interactions of portions of the zeolite lattice not directly connected to the active site.

Table 4
Effect of individual model variables (Cluster size, DFT Functional and basis set size) on predicted C_2 Dehydrogenation PES. Electronic energy barriers ($\Delta E^{\ddagger}$) at zero Kelvin are calculated using both model variables and the difference between them is reported as the barrier change. Reproduced by permission from Ref. [15].

Fixed variables	Variable in model	Change in model variable	TS3 Barrier change (kcal/mol)
T5, ωB97X-D	Basis set Size	6-31G(d,p) → 6–311++G(3df,3pd)	−5.0
T5, 6-31G(d,p)	DFT functional	B3LYP → ωB97X-D	−6.5
ωB97X-D,6-31G(d,p)	Cluster size	T5 → T437	−17.6

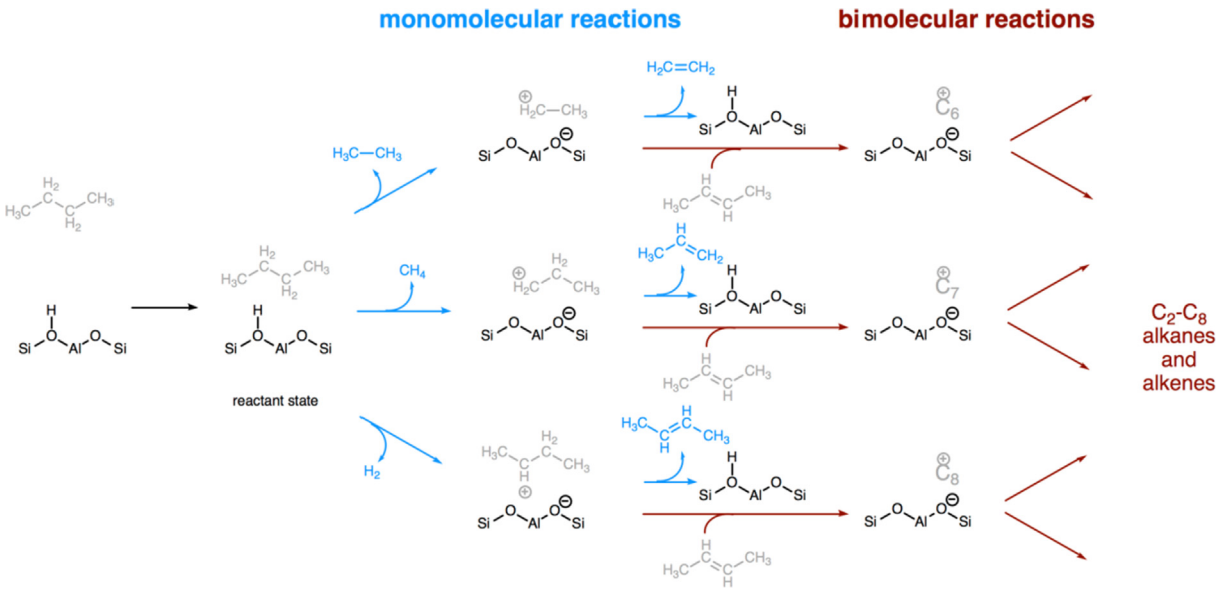

Fig. 6. Reaction mechanisms for butane cracking over Brønsted acid zeolites at low conversion (monomolecular reactions; blue) and high conversion (bimolecular reactions; red). Reproduced by permission from Ref. [6]. (For interpretation of the references to color in this figure legend, the reader is referred to the web version of this article.)

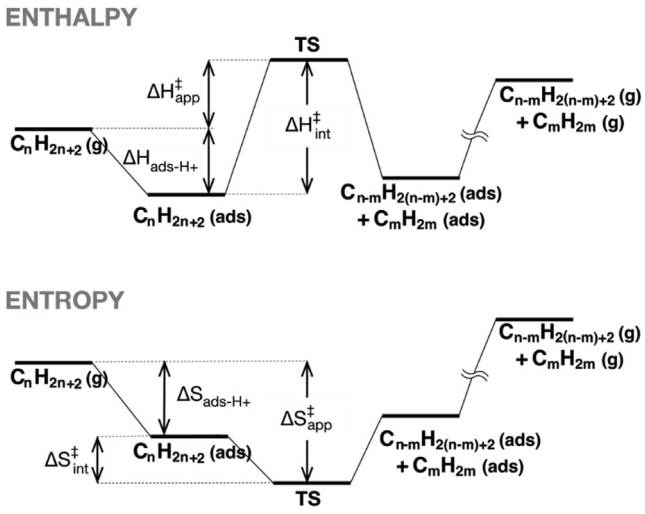

Fig. 7. Schematic enthalpy and entropy landscapes illustrating the various steps in monomolecular reactions of alkanes in a Brønsted acid zeolite: the alkane adsorbs onto an active site, is converted into an alkene and a smaller alkane (cracking, m < n) or H_2 (dehydrogenation, m = n), and the cracking or dehydrogenation products desorb from the active site. Apparent activation parameters ($\Delta H^{\ddagger}_{app}$ and $\Delta S^{\ddagger}_{app}$) extracted directly from experimental measurements are determined by both the adsorption enthalpy ($\Delta H_{ads\text{-}H+}$) and adsorption entropy ($\Delta S_{ads\text{-}H+}$) of the reactants at the Brønsted acid sites and the intrinsic activation parameters ($\Delta H^{\ddagger}_{int}$ and $\Delta S^{\ddagger}_{int}$) associated with the chemical transformation at the active site. Reproduced by permission from Ref. [6].

5.2. Effects of zeolite structure on butane cracking and dehydrogenation

Brønsted acidic protons, which compensate for the substitution of trivalent Al for tetravalent Si in the zeolite framework (≡Si-(OH)-Al≡) are the most common active sites in zeolites. The activity and selectivity of such sites depends on the acidity of the proton and on its spatial confinement [40-48]. The latter property is defined by the size and shape of the pores and channels in the zeolite framework, which are similar in dimensions to those of reactants and products and reaction transition states. One of the ways to assess the influence of zeolite structure (pore size and topology) on the intrinsic activity and selectivity of Brønsted acid sites is to measure the first-order rate coefficients for monomolecular cracking and dehydrogenation of C_2-C_4 alkanes. In a series of studies, we have shown that considerable insight into these processes can be obtained from a theoretical analysis of the roles of alkane adsorption and reaction.

5.3. Effects of proton confinement on the cracking of light alkanes

The mechanisms by which alkane cracking and dehydrogenation occur are illustrated in Fig. 6 for the case of butane [6]. At low conversion, both reactions begin with adsorption of the alkane at a Brønsted acid site. Monomolecular cracking or dehydrogenation then occurs from this reactant state and, as illustrated, can lead to a variety of products via secondary reactions at higher conversion. Fig. 7 illus-

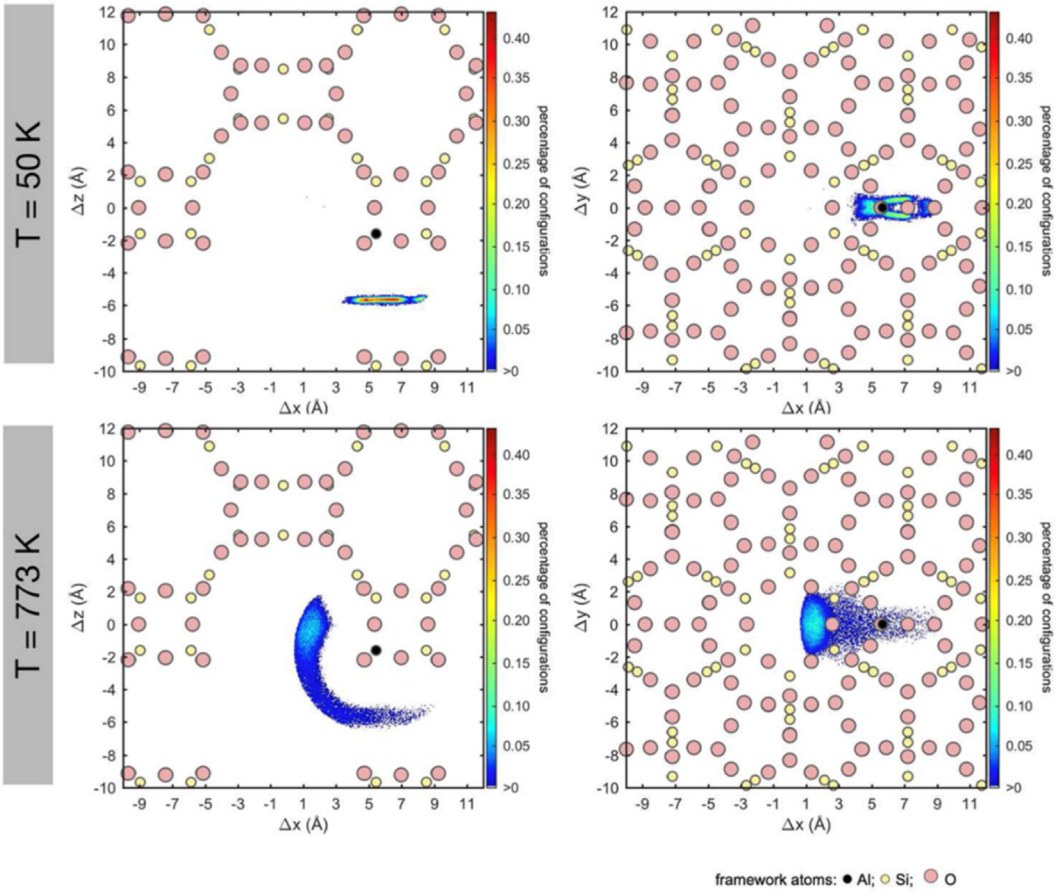

Fig. 8. Heat maps showing the distribution of C atoms of the terminal C – C bond of n-butane interacting via this bond with a Brønsted acid site at site T4 in MWW, obtained from CBMC simulations at 50 K and at 773 K. At 50 K, butane is predominantly adsorbed in the sinusoidal channel, while at 773 K, adsorption in the supercage is favored for entropic reasons. Framework atoms outside the plane represented in the heat maps have been omitted for clarity. The color scale represents the percentage of configurations in which the C atom is found within a square with side length 0.05 Å projected onto different planes. Reproduced with permission from Ref. [40].

Table 5
Thermal corrections at 773 K to $\Delta H^{\ddagger}_{app}$ and $\Delta S^{\ddagger}_{app}$ for each zeolite framework derived from adsorption thermodynamic data obtained using CBMC simulations at an Al atom in the T-sites used in the QM/MM calculations (in parentheses). Reproduced with permission from Ref. [40].

	$\Delta\Delta H_{config}$ kJ mol^{-1}	$\Delta\Delta S_{config}$ J mol^{-1} K^{-1}
TON (T2)	20	62
FER (T2)	10	64
-SVR (T19)	19	69
MFI (T12)	10	75
MEL (T4)	18	81
STF (T2)	11	76
MWW (T4)	43	86

Table 6
Topological characteristics of zeolite frameworks including number of T-atoms circumscribing the channels, pathways traced by channels, diameter of largest cavity, and percentage of pore volume present in cages. Adapted from Ref. [51].

	Channels		Cavities	
Framework type	Ring size (T-atoms)	Channel pathway	Largest cavity diameter (Å)	Pore volume in cages (%)
FER	10	straight	7.0	47
	8	straight		
MEL	10	straight	8.4	40
MFI	10	sinusoidal	7.0	26
	10	straight		
MWW	10	sinusoidal	10.3	27
	10	sinusoidal		
STF	10	straight	8.3	85
SVR	10	sinusoidal	5.7	21
	10	sinusoidal		
	10	sinusoidal		
TON	10	straight	–	0

Table 7
Adsorption equilibrium constant ($K_{ads\text{-}H+}$) and enthalpies ($H_{ads\text{-}H+}$) and entropies ($S_{ads\text{-}H+}$) of adsorption for n-butane adsorbed in a reactant state and Boltzmann averaged over all C-C bonds, determined using CBMC simulations at 773 K. Each quantity corresponds to a random distribution of Al. Adapted from Ref. [51].

Framework type	$K_{ads\text{-}H+}$	$H_{ads\text{-}H+}$	$S_{ads\text{-}H+}$
FER	0.25	−51.8	−74.2
TON	0.30	−56.1	−70.1
SVR	0.34	−47.2	−61.8
MEL	0.39	−48.4	−62.0
MFI	0.64	−49.8	−59.7
MWW	0.83	−44.7	−51.1
STF	1.21	−46.0	−49.7

trates the processes of alkane adsorption into the reactant state and the subsequent reaction in terms of the relevant changes in the enthalpy and entropy of the reactant relative to its presence in the gas phase. Since the alkane concentration within the zeolite pores is small due to the weak interaction of the alkanes with the Brønsted acid site, the occupancy of these sites ($\theta_{ads\text{-}H+}$) can be described by Henry's law [49]:

$$\theta_{ads-H+} = K_{H-H+} P_a \tag{9}$$

In Eq. (9), $K_{H\text{-}H+}$ is the Henry's law constant for alkane adsorption to the reactant state, which is defined as any configuration in which an alkane C-C bond is located within 5 Å of an Al T-atom, and P_a is the alkane partial pressure [49]. The relationship of $K_{H\text{-}H+}$ to the dimensionless thermodynamic equilibrium constant for adsorption to the reactant state, $K_{ads\text{-}H+}$, is given by [50]:

$$K_{H-H+} \equiv \frac{RT}{V_{H+} n_{H+}} K_{ads-H+} \tag{10}$$

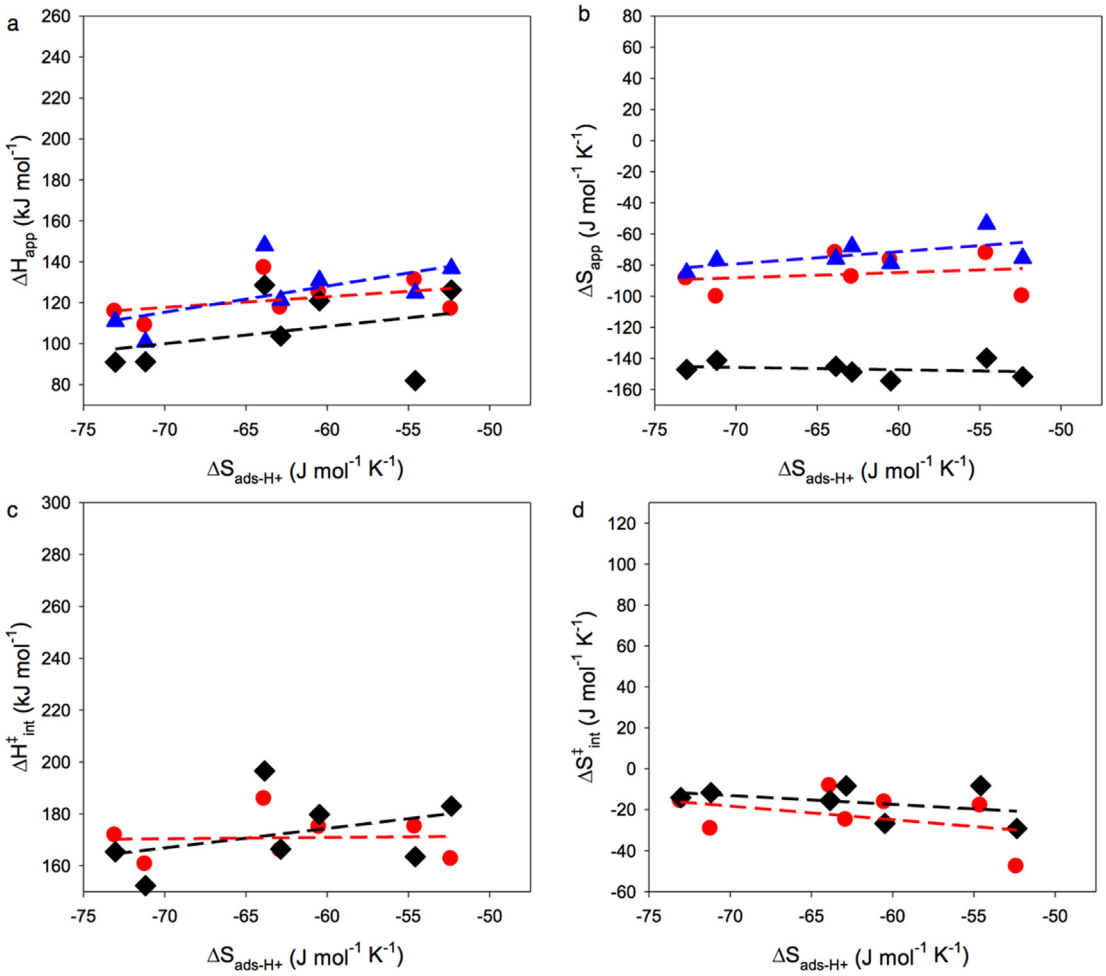

Fig. 9. Plots of apparent activation enthalpy (a) and entropy (b), and intrinsic activation enthalpy (c) and entropy (d) vs. adsorption entropy determined from CBMC simulations for central cracking of n-butane at 773 K. Experimental values (red circles taken from Ref. [52] are compared with theoretical values determined from QM/MM using the quasi-RRHO approach before (black diamonds) and after (blue triangles) adding the thermal corrections derived from CBMC simulations. Representative 95% confidence intervals for the experimental values of $\Delta H^{\ddagger}_{app}$ and $\Delta S^{\ddagger}_{app}$ are ± 7 kJ mol^{-1} and ± 9 J mol^{-1} K^{-1}. Reproduced by permission from Ref. [40]. (For interpretation of the references to color in this figure legend, the reader is referred to the web version of this article.)

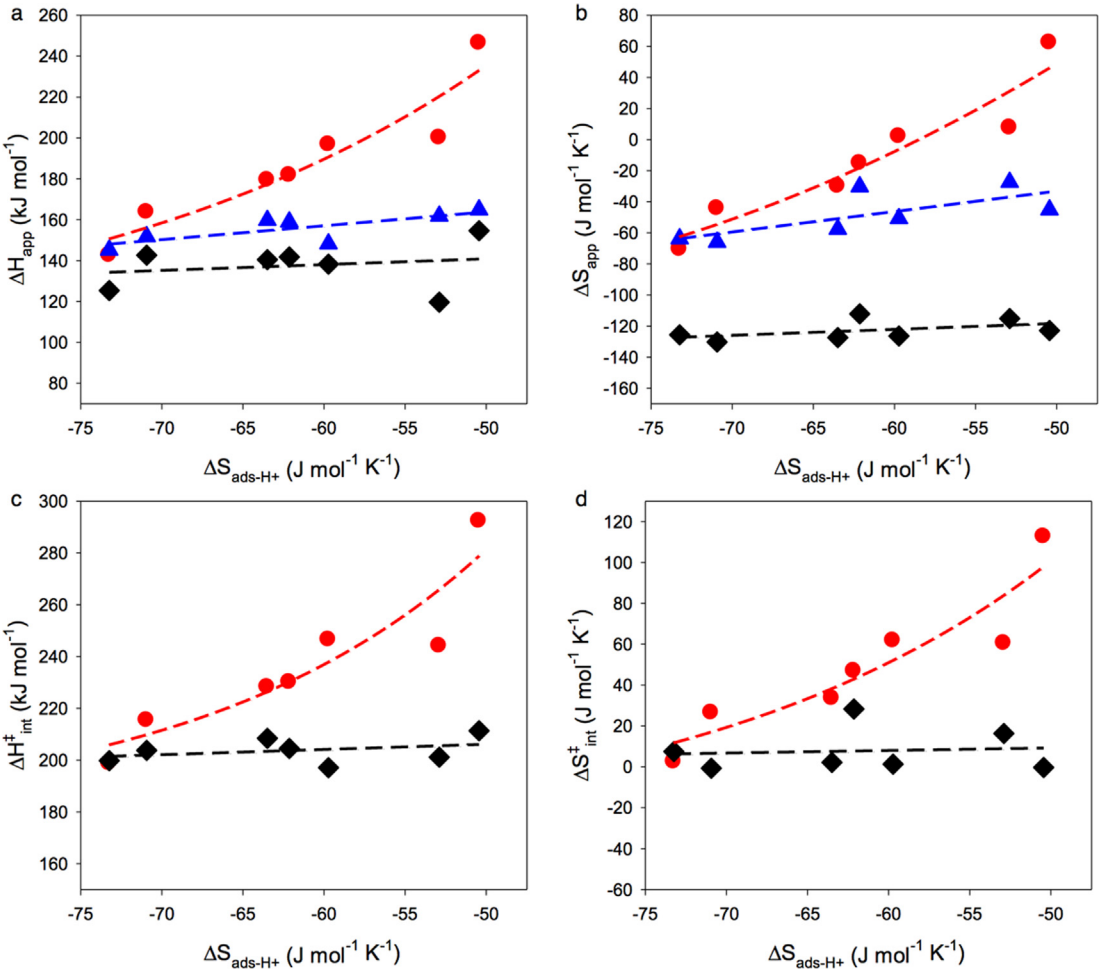

Fig. 10. Plots of apparent activation enthalpy (a) and entropy (b), and intrinsic activation enthalpy (c) and entropy (d) vs. adsorption entropy determined from CBMC simulations for methylene dehydrogenation of n-butane at 773 K. Experimental values (red circles taken from Ref. [52] are compared with theoretical values determined from QM/MM using the quasi-RRHO approach, before (black diamonds) and after (blue triangles) adding the thermal corrections derived from CBMC simulations. Representative 95% confidence intervals for the experimental values of $\Delta H^{\ddagger}_{app}$ and $\Delta S^{\ddagger}_{app}$ are ± 8 kJ mol^{-1} and ± 11 J mol^{-1} K^{-1}. Reproduced by permission from Ref. [40]. (For interpretation of the references to color in this figure legend, the reader is referred to the web version of this article.)

Table 8
Apparent enthalpy barriers ($\Delta H^{\ddagger}_{app}$) for light alkane dehydrogenation (kcal/mol) predicted using QM/MM on Ga-based sites in comparison to available experimental data measured for light alkane dehydrogenation on Ga/H-MFI. Range of reported barriers is based on measurements made between 718 and 823 K. The activation barriers reported in bold font are found to be kinetically relevant based on our energetic span analysis. Reproduced by permission from Ref. [16].

Light Alkane	Calculated $\Delta H^{\ddagger}_{app}$ (kcal/mol)			Measured $\Delta H^{\ddagger}_{app}$ (kcal/mol) [54–56]		
	$[GaH_2]^+$ (Stepwise Alkyl)	$[GaH]^{2+}$ (Carbenium)	$[GaH]^{2+}$ (Alkyl)	Ga/H-MFI	Ga/Al	Si/Al
Ethane	27.5	28.2	35.8	30.5	0.5	16
Propane	26.2	26.5	23.4	25.6	0.4	16
Butane	28.9	21.9	19.8	–	–	–
Isobutane	31.7	29.3	22.3	23.8	0.1	16.5

where V_{H+} is the volume contained within one mole of reactant state spheres of radius 5 Å and n_{H+} is the moles of protons per unit mass of zeolite. Under such circumstances, the apparent rate coefficient (k_{app}) of an elementary reaction depends on both the thermodynamics of the adsorption at the active sites ($K_{ads\text{-}H+}$) and the intrinsic rate coefficient (k_{int}) [51]:

$$k_{app} K_{ads-H+} k_{int} \tag{11}$$

Our studies have shown that the location of an Al atom in a zeolite framework and the overall framework structure affect the values of k_{app} and its components, $K_{ads\text{-}H+}$ and k_{int}. The impact of zeolite structure can be established from calculations of the apparent activation enthalpy and entropy ($\Delta H^{\ddagger}_{app}$ and $\Delta S^{\ddagger}_{app}$). This approach begins by expressing $\Delta H^{\ddagger}_{app}$ and $\Delta S^{\ddagger}_{app}$ in terms of their component parts:

$$\Delta H^{\ddagger}_{app} = \Delta H_{ads\text{-}H+} + \Delta H^{\ddagger}_{int} \tag{12}$$

$$\Delta S^{\ddagger}_{app} = \Delta S_{ads\text{-}H+} + \Delta S^{\ddagger}_{int} \tag{13}$$

Here $\Delta H_{ads\text{-}H+}$ and $\Delta S_{ads\text{-}H+}$ are the enthalpy and entropy, respectively, of alkane adsorption into the reactant state and $\Delta H^{\ddagger}_{int}$ and $\Delta S^{\ddagger}_{int}$ are the enthalpy and entropy, respectively, of activation for an alkane molecule in the reactant state. Values of $\Delta H_{ads\text{-}H+}$ and $\Delta S_{ads\text{-}H+}$ were obtained using a theoretical approach based on configurational-bias Monte Carlo (CBMC) simulations, whereas values $\Delta H^{\ddagger}_{int}$ and $\Delta S^{\ddagger}_{int}$ were determined from DFT calculations using a QM/MM approach.

Analysis of the CBMC simulations shows that at 773 K, a typical temperature for alkane cracking and dehydrogenation, the entropy and enthalpy of the reactant state are underestimated relative to the values predicted from DFT calculations of the internal energy combined with estimates of the vibrational contribution to the enthalpy and entropy based on quasi-RRHO calculations of vibrational frequencies [40]. The reason for this is that at elevated temperatures, the reactant state occupies several configurations close to that predicted by DFT for the stationary point at 0 K. The heat map presented in Fig. 8 for zeolite MWW illustrates this point. The differences in the values of the enthalpy and entropy of adsorption into the reactant state at 773 K calculated by CBMC and DFT/quasi-RRHO, $\Delta\Delta H_{config}$ and $\Delta\Delta S_{config}$, are given in Table 5 for different zeolites. What is seen is that the values of $\Delta\Delta H_{config}$ are 10–43 kJ mol^{-1} and the values of $\Delta\Delta S_{config}$ are 62–86 J mol^{-1} K^{-1}, depending on the zeolite structure.

Cracking and dehydrogenation of butane in zeolites TON, FER, -SVR, MFI, MEL, STF and MWW, all of which feature 10-ring channels (see Table 6), were analyzed. These zeolite frameworks form a good basis for identifying the effects of confinement on monomolecular reaction kinetics because they represent a wide range of Brønsted-acid site confinement. The level of confinement for each zeolite within a given channel topology (e.g., straight vs sinusoidal channels) is described by the entropy of adsorption of n-butane adsorbed in the reactant state. Table 7 shows that $\Delta S_{ads\text{-}H+}$ is a good descriptor of the equilibrium constant for alkane adsorption from the gas phase to the reactant state, $K_{ads\text{-}H+}$.

Figs. 9 and 10 show that values of $\Delta H^{\ddagger}_{app}$ and $\Delta S^{\ddagger}_{app}$ calculated using the quasi-RRHO approach are underestimated, especially for the less confining zeolites (e.g., STF). Adding the CBMC corrections (see Table 5) significantly improves the agreement between theoretical and experimental values of $\Delta H^{\ddagger}_{app}$ and $\Delta S^{\ddagger}_{app}$ for all zeolites, which indicates that the configurational enthalpy and entropy of the transition state are

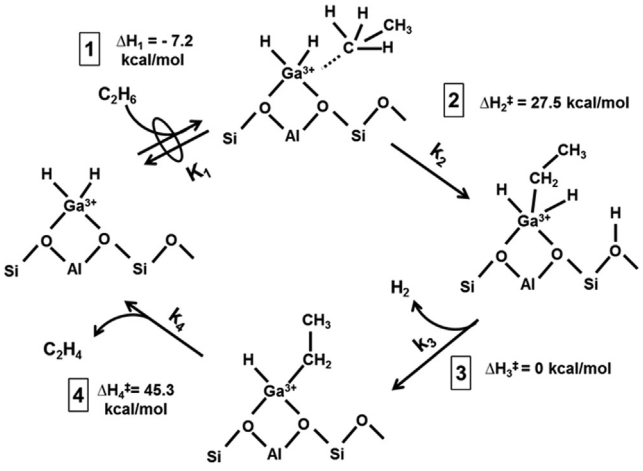

Scheme 1. Proposed elementary steps for C_2H_6 dehydrogenation over $[GaH_2]^+$ cations via the alkyl mechanism. Activation enthalpies are denoted as $\Delta H^{\ddagger}$. Reproduced by permission from Ref. [57]

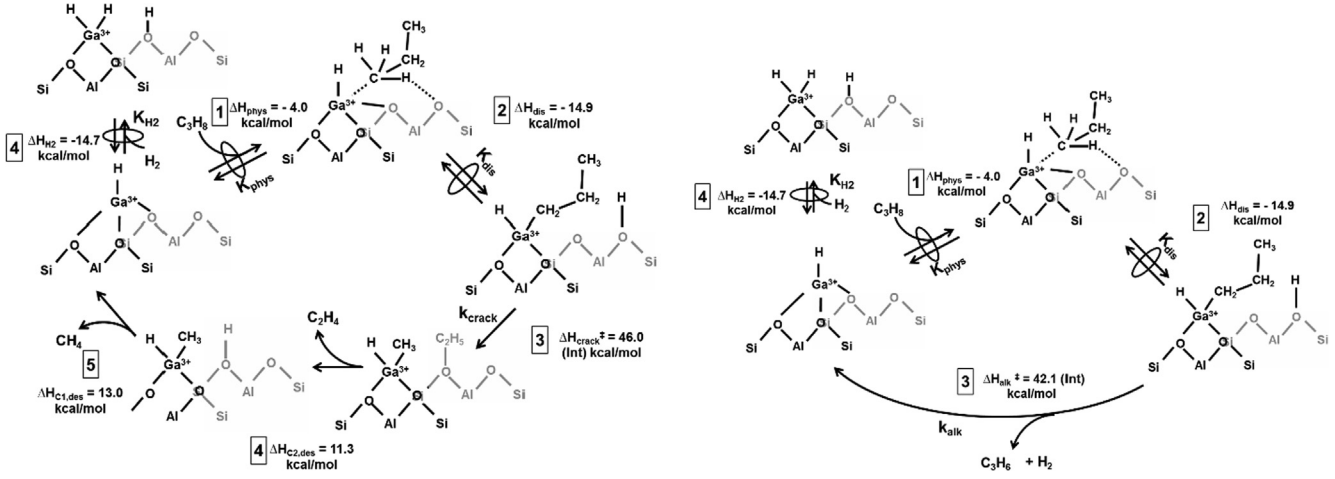

Scheme 2. Proposed elementary steps for C_3H_8 dehydrogenation (left) and cracking (right) of over $[GaH]^{2+}$ sites by the alkyl mechanism. Enthalpies (adsorption, reaction and activation) for each step are shown here with respect the enthalpy of the initial structure in the step. For each structure, framework atoms that are faded reflect cation-exchange sites that are behind the image plane for non-faded cation-exchange sites. Cations coordinated to the faded cation-exchange sites are also behind the image plane but have not been faded for visual purposes. Reproduced by permission from Ref. [57].

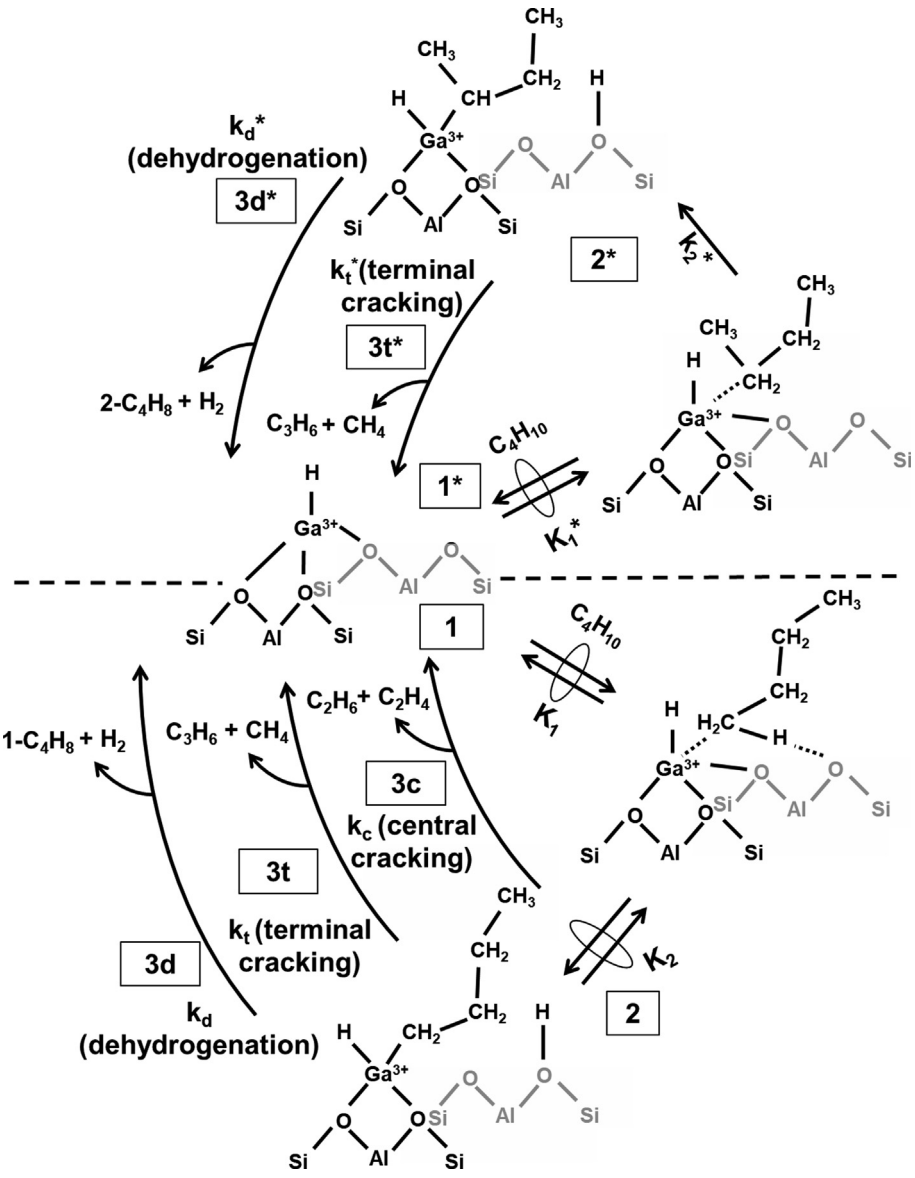

Scheme 3. Proposed elementary steps for *n*-C_4H_{10} dehydrogenation and both terminal and central cracking over $[GaH]^{2+}$ cations. For each structure, framework atoms that are faded reflect cation-exchange sites that are behind the image plane for non-faded cation-exchange sites. Cations coordinated to the faded cation-exchange sites are also behind the image plane but have not been faded for visual purposes. Reproduced by permission from Ref. [58].

fairly similar to those of the reactant state, consistent with the early character of the central cracking transition state [52]. By contrast, for dehydrogenation, adding the CBMC corrections only improves the agreement between $\Delta H^{\ddagger}_{app}$ and $\Delta S^{\ddagger}_{app}$ from theory and experiment for the zeolites with the most confining structures (e.g., TON and FER). As the confinement decreases, theory increasingly underestimates the experimental values of $\Delta H^{\ddagger}_{app}$ and, more strongly, $\Delta S^{\ddagger}_{app}$. This deviation is attributed to the fact that dehydrogenation occurs via a late transition state, and the CBMC corrections derived from the reactant state fail to account for the uncorrelated rotations and translations of the product-like fragments making up the transition state [40,52].

5.4. Role of Ga cations in the dehydrogenation of light alkanes over Ga/H-MFI

Ga-exchanged H-MFI zeolites are highly active for the dehydrogenation of light alkanes; however, both the nature of the active gallium species and the associated dehydrogenation mechanism have been difficult to establish. Prior studies have shown that alkane dehydroaromatization begins with alkane dehydrogenation to form alkenes, which then undergo oligomerization and dehydrogenation of the resulting products to produce aromatic compounds. Since alkane dehydrogenation is the first step in the overall dehydroaromatization process and Ga cations are the active center for promoting this initial reaction, considerable effort has been devoted to identifying the composition and structure of extra-framework Ga cations and their role in alkane dehydrogenation. Characterization of Ga cations in MFI by various experimental methods have suggested that extra-framework, exchanged Ga cations can exist as mononuclear (Ga^+, $[GaH]^{2+}$, and $[GaH_2]^+$, $[GaO]^+$, and $[GaHOH]^+$) and binuclear ($[Ga_2O_2]^{2+}$ and ($[Ga_2O_2H_2]^{2+}$) species; theoretical support for these species has been reported as well (see Refs. [16,53]) and references cited therein).

Table 9
Experimentally measured activation enthalpies for C_2H_6 dehydrogenation over Ga/H-MFI (Ga/Al = 0.5) for first- and zero-order rate coefficients. Also shown are theoretically predicted values of activation enthalpies for Steps 2 and 4 from Scheme 1. Adapted from Ref. [58].

Enthalpy (kcal/mol)	Dehydrogenation Experiment	Dehydrogenation Theory
$\Delta H^{\ddagger}_{app}$	25.5 ± 4.7	27.5
$\Delta H^{\ddagger}_{int}$	35.9 ± 3.5	45.3

Table 10
Apparent and intrinsic activation enthalpies for C_3H_8 dehydrogenation and cracking over Ga/H-MFI (Ga/Al = 0.2. Also shown are theoretically predicted activation enthalpies for C_3H_8 dehydrogenation and cracking over $[GaH]^{2+}$ via alkyl and carbenium mechanisms and for the enthalpies of dissociative adsorption for C_3H_8 and H_2. Reported uncertainties reflect 95% confidence intervals. Adapted from Ref. [58].

Enthalpy (kcal/mol)	Dehydrogenation Experiment	Dehydrogenation Theory	Cracking Experiment	Cracking Theory
$\Delta H^{\ddagger}_{app}$	19.0 ± 6.0	23.2	26.5 ± 0.3	27.1
$\Delta H^{\ddagger}_{int}$	34.6 ± 1.0	42.1	42.0 ± 4.7	46.0

Table 11
Experimentally measured apparent ($\Delta H^{\ddagger}_{app}$) enthalpies for *n*-$C_4H_{10}$ dehydrogenation and both terminal and central cracking over Ga/H-MFI (Ga/Al = 0.2). Also shown are theoretically predicted values of these quantities for dehydrogenation via [n-C_4H_9-GaH]-H^+ cation pairs. Adapted from Ref. [58].

Enthalpy (kcal/mol)	Dehydrogenation		Terminal cracking		Central cracking	
	Experiment	Theory	Experiment	Theory	Experiment	Theory
$\Delta H^{\ddagger}_{app}$	17.5 ± 4.7	19.7	19.9 ± 0.3	22.4	16.8 ± 0.9	14.9

We have carried out QM/MM calculations using a range-separated and dispersion-corrected ωB97X-D functional, to analyze the energetics of light alkane dehydrogenation and cracking over Ga/H-MFI [16]. This effort was informed by our experimental work, which showed that for Ga/Al ratios below about 0.3, Ga^{3+} cations are associated with proximate pairs of cation-exchange sites as either $[GaH]^{2+}$ cations for Ga/Al = 0.1 and as both $[GaH]^{2+}$ cations and $[Ga(H)_2]^+/H^+$ cation pairs for higher Ga/Al ratios [53]. The molecular mechanics part of our approach captures the long-range effects of coulombic and dispersive interactions due to atoms in the extended framework. The rate-determining TS (RDTS) was identified by analysis of the free energy landscape for each mechanism, using the energetic span model (see above). Our analysis revealed that for reduced Ga/H-MFI, univalent and divalent gallium hydrides: $[GaH_2]^+$ and $[GaH]^{2+}$ respectively, are more active for ethane dehydrogenation than H^+ sites and Ga^+ sites. $[GaH]^{2+}$ sites emerged consistently as the most active sites for light alkane dehydrogenation, providing significant enthalpic stabilization for C-H cleavage TSs via alkyl and carbenium dehydrogenation routes. By contrast, carbenium-like C-H cleavage TSs occurring on Brønsted acid sites were found to be enthalpically less favorable due to their limited electronic interactions with framework O atoms and H^+ sites. As shown in Table 8, activation enthalpy barriers for alkane dehydrogenation determined using the energetic span analysis are in good agreement with those measured experimentally. Examination of the entropy of activation reveals that constrained TSs become less favorable in free energy with increasing chain length. We have also found that an increase in enthalpic favorability of the alkyl mechanism is observed with increasing chain length for the TS responsible for the second C-H cleavage step leading to alkene formation. (See Scheme 1).

Analysis of the mechanism of light alkane dehydrogenation and cracking over Ga/H-MFI

Our experimental studies of ethane, propane, and butane dehydrogenation and cracking have revealed that both $[GaH]^{2+}$ and $[GaH_2]^+$ cations are equally active for ethane dehydrogenation, only $[GaH]^{2+}$ is active for propane and butane dehydrogenation and cracking [56-58]. Analysis of the free energy landscape for each of these reactants shows that ethane dehydrogenation occurs preferentially via a carbenium mechanism over $[GaH]^{2+}$ cations or via a stepwise alkyl mechanism over $[GaH_2]^+$ cations. By contrast both propane and butane dehydrogenation and cracking occur preferentially via an alkyl mechanism on $[GaH]^{2+}$ cations. These mechanisms are illustrated in Schemes 2-4.

For each alkane, reaction begins with the reversible adsorption of the alkane followed by dissociation of a C-H bond. In the case of ethane of both ethane and propane, the latter step involves cleavage of a C-H bond in the methyl group. While cleavage of methylene C-H bond could occur for propane this step is not preferred from a free energy of activation perspective compared to cleavage of the methyl C-H bond. By contrast, for butane both processes can occur simultaneously. In all cases, bonding of the alkyl fragment is preferentially to the Ga cation and an anion, whereas the H released from the hydrocarbon bonds as a proton to a zeolite framework O atom adjacent to an Al atom. The alkyl anion then undergoes dehydrogenation to form H_2 and the corresponding alkene. For ethane dehydrogenation, the rate-limiting step is the cleavage of a methyl group C-H bond in adsorbed ethane; whereas for propane and butane this step is quasi-equilibrated and the rate-limiting step is the loss of an H atom from the alkyl anion. Propane and butane cracking also involves the alkyl fragment, and the rate limiting step in this case is cleavage of a C-C bond. In the case of butane, this last step can lead to either central or terminal cracking.

Experimental and theoretical values of the apparent activation enthalpies for dehydrogenation and cracking for all are presented in Tables 9-11 for ethane, propane, and butane, respectively. For all three alkanes, the apparent activation energy for dehydrogenation agrees reasonably well with that observed experimentally. It is also seen that the magnitude of the activation enthalpy decreases slightly with increasing chain length consistent with what is observed experimentally. For propane, the activation enthalpy for cracking to ethene/methane predicted and observed are in good agreement, as is the higher activation enthalpy for cracking than dehydrogenation. In the case of butane, the predicted and observed activation energies for central and terminal cracking to ethene/ethane and propene/methane agree reasonably well, as doe the observation that the activation enthalpy for central cracking is lower than that for terminal cracking. We also note that the theo-

retical analysis correctly predicts that the activation enthalpy for ethane cracking to ethene/methane is higher than that for butane cracking to propene/methane. Thus, in summary, the theoretical model used to analyze the energetics of light alkane dehydrogenation and cracking on Ga/H-MFI correctly captures the effects of the active form of Ga cation for each alkane and the influence of alkane chain length.

6. Conclusions and perspectives

We have shown that a hybrid QM/MM model can be used to conduct meaningful theoretical analyses of the kinetics of zeolite catalyzed reactions of hydrocarbons. The first requirement is that the cluster representing active site in the zeolite and a portion of the active center in the zeolite and the adjacent portions of the framework must be sufficiently large to capture both bonding and non-bonding interactions between the active center and reactants, intermediates, products. Accurate QM calculations for this cluster and all adsorbate atoms must be done using a high-quality density functional such as the range-separated dispersion-corrected hybrid GGA ωB97X-D to accurately describe non-covalent interactions, barrier heights and kinetics. Moreover, the QM cluster must be embedded in a much larger cluster (one having 100 s at T atoms) to account for the long-range effects of van der Waals and coulombic interactions to the active part of the zeolite and the adsorbed species with the extended zeolite framework. We have shown that when such conditions are observed, QM/MM calculations can predict adsorption enthalpies with good accuracy relative to measurements made at low temperatures (<373 K). At higher temperatures, CBMC calculations indicate that adsorption enthalpies can decrease by 2.5 kcal/mol to 10 kcal/mol relative to values predicted from QM/MM calculations.

We have also shown that accurate predictions of adsorption and activation entropies remains a challenge. The rigid-rotor harmonic oscillator approximation for the adsorbate substantially over predicts the entropy of adsorption. Some improvement can be made by adopting the quasi-RRHO approximation which treats low frequency modes as a combination of vibrations and hindered rotations. However, even this approximation is not adequate. CBMC estimates demonstrate that the entropy loss upon adsorption is overestimated by this approximation by as much as 15–20 cal/mol K, and that the degree of correction decreases as the extent of adsorbate confinement increases (see Table 5). We note that while the correction obtained from CBMC can be extended to early transition states for first order reactions, in which that transition state resembles the reactant state (e.g., cracking), it is inadequate for late transition states for which the transition state structure resembles the product state (e.g., dehydrogenation). We also note that the problem of determining the entropy becomes more severe as the degree of confinement by the zeolite framework decreases. The treatment of reactions involving such loose transition states in large-pore zeolites is an ongoing research challenge. In a recent perspective, Rousseau and coworkers have discussed the need for advanced methodologies to account for anharmonicity and its effects on entropy in heterogeneous catalysis, specifically for systems involving supported nanoparticles, solid/liquid interfaces and nanoporous solids such as zeolites [59].

In a similar approach to the one followed by Van der Mynsbrugge et al. [6] one might consider attempting to derive configurational corrections for reactions with a late transition state based on the product state instead of the reactant state. While this may certainly be possible in some cases, this is not an option in the case of alkane dehydrogenation, since the interaction of the alkene formed in this reaction with the acid site cannot be described with the classical force fields used in CBMC simulations, and a first-principles approach is required. Alkenes rapidly undergo protonation, even at low temperatures, and the nature of the intermediates formed under reaction temperatures remains unclear. Recent studies using ab initio molecular dynamics have shown that alkenes interacting with Brønsted acid sites can form a π-complex, a carbenium ion or a covalently bound alkoxide, depending on the temperature, the chain length of the alkene and the degree of branching [60,61].

The products formed immediately after crossing the transition state for alkane cracking or dehydrogenation are metastable intermediates that are separated from more stable species by relatively small barriers that are easily overcome at reaction temperatures. Zimmerman et al. have employed quasi-classical trajectory simulations with initial nuclear velocities derived from the QM populations of the vibrational modes in the transition state at reaction temperature to investigate the non-equilibrium pathways through which the carbenium ion intermediates formed by the protonation of C-C bonds in n-pentane evolve into a variety of cracking products. The prevailing pathways, which ultimately determine the experimentally observed product selectivity for n-pentane cracking in H-MFI, were shown to deviate significantly from the potential energy surface at 0 K obtained from static electronic structure calculations [62].

With the increasing availability of more powerful computers, several research groups have started to explore the use of *ab initio* molecular dynamics (AIMD) methods [63] on zeolite systems [59,60,64-70]. While molecular dynamics methods provide natural access to the free energy surfaces at reaction temperatures, the time scale that can be studied in an AIMD simulation is in the order of ~ 100 ps. Even for chemical reactions with a high turnover frequency, the probability of the reaction occurring in a given 100 ps window is extremely low. To enable the study of such rare events with molecular dynamics, techniques are required to enhance their sampling by forcing the system to cross the free energy barrier associated with the reaction of interest [71-77]. The success of a metadynamics simulation depends on the choice of collective variables along which the bias potential is applied to the system, which in turn requires prior knowledge of the reaction mechanism. More recently, transition path sampling (TPS) has received attention as a bias-free alternative [78]. TPS combines AIMD with MC moves to randomly generate an ensemble of transition paths between reactants and products, from which the free energy barrier and rate constant can be derived. Bučko and coworkers have demonstrated the potential of TPS for elucidating the nature of reaction intermediates involved in zeolite-catalyzed alkane dehydrogenation at operating temperatures [79]. While their computational cost remains too high to enable routine applications, these methods offer great promise for future research efforts in zeolite catalysis.

A different approach to extending the time scales accessible in molecular dynamics simulations is to reduce the computational cost per time step while maintaining accuracy. Force fields derived from high-level ab initio data are a promising alternative to force fields derived from experimental data, which often perform poorly for the description of porous materials [80]. Recently, Sholl et al. have developed a force field that describes the adsorption and diffusion of paraffins and small molecules with siliceous zeolites with coupled-cluster accuracy [81].

7. Personal acknowledgement

I first met Michel Boudart at an ACS in San Francisco during the mid-1970′s, at a time when an increasing part of my research program was becoming devoted to catalysis. Till then I had only heard about him from my colleagues. What impressed me immediately, and even

more subsequently, was his deep understanding of kinetics and his keen eye for inconsistencies in work that was being presented. As my own work on catalysis became the central focus of my research program, I had more and more opportunity to become familiar with Michel, both as a scholar and as a person. From reading his book on the kinetics of catalyzed reactions and from my many discussions with him, I came to appreciate the importance of kinetics and its central place in the field. In fact, it was Michel who made me realize that the most sensitive indicators of changes in the composition and structure of a catalyst are their effects on the catalyst activity and selectivity, and in particular on specific elementary processes. The early appreciation of these facts has served me well throughout my career, and I am forever grateful to Michel for teaching me this important lesson.

Declaration of Competing Interest

The authors declare that they have no known competing financial interests or personal relationships that could have appeared to influence the work reported in this paper.

Acknowledgements

This work was supported by a grant from Chevron Energy Technology Co. ATB would also like to thank Prof. Martin Head-Gordon for his contributions to many of the publications on which this work is based and for a highly fruitful collaboration spanning two decades.

References

[1] https://www.grandviewresearch.com/industry-analysis/catalyst-market.
[2] J.A. Dumesic, D.F. Rudd, L.M. Aparico, J.E. Rekoske, A.A. Treviño, The Microkinetics of Heterogeneous Catalysis, American Chemical Society, Washington, DC, 1993.
[3] A.N. Mlinar, P.M. Zimmerman, F.R. Celik, M. Head-Gordon, A.T. Bell, Effects of Brønsted-acid site proximity on the oligomerization of propene in H-MFI, J. Catal. 288 (2012) 65–73.
[4] A.T. Bell, M. Head-Gordon, Quantum Mechanical Modeling of Catalytic Processes, Annu. Rev. Chem. Biomol. Eng. 2 (1) (2011) 453–477.
[5] E.A. Pidko, Toward the Balance between the Reductionist and Systems Approaches in Computational Catalysis: Model versus Method Accuracy for the Description of Catalytic Systems, ACS Catal. 7 (2017) 4230–4234.
[6] J. Van der Mynsbrugge, A. Janda, L.C. Lin, V. Van Speybroeck, M. Head-Gordon, A.T. Bell, Understanding Brønsted-Acid Catalyzed Monomolecular Reactions of Alkanes in Zeolite Pores by Combining Insights from Experiment and Theory, ChemPhysChem 19 (2018) 341–358.
[7] M. Sierka, J. Sauer, Structure and reactivity of silica and zeolite catalysts by a combined quantum mechanics shell-model potential approach based on DFT, Faraday Discussions. 106 (1997) 41–62.
[8] T. Maihom, B. Boekfa, J. Sirijaraensre, T. Nanok, M. Probst, J. Limtrakul, Reaction Mechanisms of the Methylation of Ethene with Methanol and Dimethyl Ether over H-ZSM-5: An ONIOM Study, J Phys Chem C. 113 (16) (2009) 6654–6662.
[9] T. Maihom, P. Pantu, C. Tachakritikul, M. Probst, J. Limtrakul, Effect of the Zeolite Nanocavity on the Reaction Mechanism of n-Hexane Cracking: A Density Functional Theory Study, The Journal of Physical Chemistry C. 114 (2010) 7850–7856.
[10] J. Van der Mynsbrugge, M. Visur, U. Olsbye, P. Beato, M. Bjørgen, V. Van Speybroeck, S. Svelle, Methylation of benzene by methanol: Single-site kinetics over H-ZSM-5 and H-beta zeolite catalysts, Journal of Catalysis. 292 (2012) 201–212.
[11] J. Van der Mynsbrugge, J. De Ridder, K. Hemelsoet, M. Waroquier, V. Van Speybroeck, Van Speybroeck, Enthalpy and Entropy Barriers Explain the Effects of Topology on the Kinetics of Zeolite-Catalyzed Reactions, Chemistry – A, European Journal. 19 (35) (2013) 11568–11576.
[12] M. Rybicki, J. Sauer J. Am. Chem. Soc. 140 (2018) 18151–18161.
[13] F. Berger, M. Rybicki, J. Sauer, J. Catal. 395 (2021) 117–128.
[14] H. Lin, D.G. Truhlar, QM/MM: What have we learned, where are we, and where do we go from here?, Theor Chem. Acc. 117 (2007) 185–199.
[15] E. Mansoor, J. Van der Mynsbrugge, M. Head-Gordon, A.T. Bell, Catal Today 312 (2018) 51–65.
[16] E. Mansoor, M. Head-Gordon, A.T. Bell, Computational Modeling of the Nature and Role of Ga Species for Light Alkane Dehydrogenation, ACS Catal. 8 (2018) 6146–6162.
[17] W. Kohn, L.J. Sham, Self-Consistent Equations Including Exchange and Correlation Effects, Phys. Rev. 140 (4A) (1965) A1133–A1138.
[18] N. Mardirossian, M. Head-Gordon, Thirty years of density functional theory in computational chemistry: an overview and extensive assessment of 200 density functionals, Mol. Phys. 115 (2017) 2315–2372.
[19] A.L. Dewyer, A.J. Argüelles, P.M. Zimmerman, Methods for exploring reaction space in molecular systems, Wiley Interdiscip. Rev. Comput. Mol. Sci. 8 (2) (2018) e1354, https://doi.org/10.1002/wcms.2018.8.issue-210.1002/wcms.1354.
[20] A. Behn, P.M. Zimmerman, A.T. Bell, M. Head-Gordon, Efficient exploration of reaction paths via a freezing string method, J. Chem. Phys. 135 (22) (2011) 224108, https://doi.org/10.1063/1.3664901.
[21] G. Piccini, M. Alessio, J. Sauer, Y. Zhi, Y. Liu, R. Kolvenbach, A. Jentys, J.A. Lercher, Accurate adsorption thermodynamics of small alkanes in zeolites. Ab initio theory and experiment for H-chabazite, J. Phys. Chem. C 119 (2015) 6128–6137.
[22] Y.-P. Li, A.T. Bell, M. Head-Gordon, Thermodynamics of Anharmonic Systems: Uncoupled Mode Approximations for Molecules, J. Chem. Theory Comp. 12 (2016) 2861–2870.
[23] V.A. Lynch, S.L. Mielke, D.G. Truhlar, Accurate vibrational-rotational partition functions and standard-state free energy values for H_2O_2 from Monte Carlo path-integral calculations, J. Chem. Phys. 121 (11) (2004) 5148–5162.
[24] V.A. Lynch, S.L. Mielke, D.G. Truhlar, High-Precision Quantum Thermochemistry on Nonquasiharmonic Potentials: Converged Path-Integral Free Energies and a Systematically Convergent Family of Generalized Pitzer−Gwinn Approximations, J Phys Chem. 109 (2005) 10092–10099.
[25] S.A. Kozuch, Refinement of Everyday Thinking: The Energetic Span Model for Kinetic Assessment of Catalytic Cycles, Wiley Interdiscip. Rev. Comput. Mol. Sci. 2 (2012) 795–815.
[26] S. Kozuch, S. Shaik, How to Conceptualize Catalytic Cycles? The Energetic Span Model, Acc. Chem. Res. 44 (2011) 101–110.
[27] S. Kozuch, J.M.L. Martin, Turning Over, Definitions in Catalytic Cycles. ACS Catal. 2 (2012) 2787–2794.
[28] S. Kozuch, S. Shaik, A Combined Kinetic-Quantum Mechanical Model for Assessment of Catalytic Cycles: Application to Cross-Coupling and Heck Reactions, J. Am. Chem. Soc. 128 (2006) 3355–3365.
[29] P.M. Zimmerman, M. Head-Gordon, A.T. Bell, Selection and Validation of Charge and Lennard-Jones Parameters for QM/MM Simulations of Hydrocarbon Interactions with Zeolites, J. Chem. Theory Comp. 7 (2011) 1695–1703.
[30] J. Gomes, P.M. Zimmerman, M. Head-Gordon, A.T. Bell, Accurate Prediction of Hydrocarbon interactions with Zeolites Utilizing improved Exchange-Correlation Functionals and QM/MM Methods: Benchmark Calculations of Adsorption Enthalpies and Application to Ethene Methylation by Methanol, J. Phys. Chem. C 116 (2012) 15406–15414.
[31] Y.P. Li, J. Gomes, S. Mallikarjun Sharada, A.T. Bell, M. Head-Gordon, Improved Force Field Parameters for QM/MM Simulations of the Energies of Adsorption for Molecules in Zeolites and a Free Rotor Correction to the Rigid Rotor Harmonic Oscillator Model for Adsorption Enthalpies, J. Phys. Chem. C 119 (2015) 1840–1850.
[32] S. Grimme, Supramolecular binding thermodynamics by dispersion-corrected density functional theory, Chem.–A Euro, J. 18 (2012) 9955–9964.
[33] J. Gomes, Theoretical Simulations of Zeolite-Catalyzed Reactions Ph.D. Thesis, University of California, Berkeley, CA, 2015.
[34] J.A. Dunne, M. Rao, S. Sircar, R.J. Gorte, A.L. Myers, Calorimetric Heats of Adsorption and Adsorption Isotherms. 2. O2, N2, Ar, CO2, CH4, C2H6, and SF6 on Na-X, H-ZSM-5, and Na-ZSM-5 Zeolites, Langmuir 12 (24) (1996) 5896–5904.
[35] M. Tarek, R. Kahn, E.C. de Lara, Modelization of Experimental Isotherms of N- Alkanes in NaX Zeolite, Zeolites 15 (1995) 67–72.
[36] O.M. Dzhigit, A.V. Kiselev, T.A. Rachmanova, Henry's Constants, Isotherms and Heats of Adsorption of Some Hydrocarbons in Zeolites of Faujasite Type with Different Content of Sodium Cations, Zeolites 4 (1984) 389–397.

[37] V.B. Kazansky, I.R. Subbotina, N. Rane, R.A. van Santen, E.J.M. Hensen, On two alternative mechanisms of ethane activation over ZSM-5 zeolite modified by Zn^{2+} and $Ga1^{+}$ cations, Phys. Chem. Chem. Phys. 7 (16) (2005) 3088, https://doi.org/10.1039/b506782k.
[38] M.S. Pereira, A.M. da Silva, M.A.C. Nascimento, Effect of the Zeolite Cavity on the Mechanism of Dehydrogenation of Light Alkanes over Gallium-Containing Zeolites, J. Phys. Chem. C 115 (20) (2011) 10104–10113.
[39] E. Pidko, V. Kazansky, E. Hensen, R. van Santen, A comprehensive density functional theory study of ethane dehydrogenation over reduced extra-framework gallium species in ZSM-5 zeolite, J. Catal. 240 (1) (2006) 73–84.
[40] J. Van der Mynsbrugge, A. Janda, S. Mallikarjun Sharada, L.-C. Lin, V, Van Speybroeck, M. Head-Gordon, A. T. Bell, Theoretical Analysis of the Influence of Pore Geometry on Monomolecular Cracking and Dehydrogenation of n-Butane in Brønsted Acidic Zeolites, ACS Catal. 7 (2017) 2685–2697.
[41] B. Smit, T.L.M. Maesen, Towards a molecular understanding of shape selectivity, Nature 451 (2008) 671–678.
[42] W. O. Haag, R. M. Dessau, The Active Site of Acidic Aluminosilicate Catalysts. Proceedings-International Congress on Catalysis, 8th, Verlag Chemie: Weinheim, Berlin, 1984, Vol. 2, pp. 305–316.
[43] S. Kotrel, H. Knözinger, B.C. Gates, The Haag-Dessau mechanism of protolytic cracking of alkanes, Micro. Meso. Mater. 35–36 (2000) 11–20.
[44] H. Konno, T. Okamura, T. Kawahara, Y. Nakasaka, T. Tago, T, Masuda, Kinetics of n-hexane cracking over ZSM-5 zeolites–effect of crystal size on effectiveness factor and catalyst lifetime, Chem. Eng. J. 207–208 (2012) 490–496.
[45] P. Voogd, H. Van Bekkum, Limitation of n-hexane and 3-methylpentane conversion over zeolite ZSM-5 by intracrystalline diffusion, Appl. Catal. 59 (1990) 311–331.
[46] W.O. Haag, R.M. Lago, P.B. Weisz, Transport and reactivity of hydrocarbon molecules in a shape-selective zeolite, Faraday Discuss. Chem. Soc. 72 (1981) 317–330.
[47] A. Janda, A.T. Bell, Effects of Si/Al Ratio on the Distribution of Framework Al and on the Rates of Alkane Monomolecular Cracking and Dehydration in H-MFI, J. Am. Chem. Soc. 135 (2013) 19193–19207.
[48] R. Gounder, E. Iglesia, Catalytic Consequences of Spatial Constraints and Acid Site Location for Monomolecular Alkane Activation on Zeolites, J. Am. Chem. Soc. 131 (2009) 1958–1971.
[49] A. Janda, B. Vlaisavljevich, L.-C. Lin, S. Mallikarjun Sharada, B. Smit, M. Head-Gordon, A.T. Bell, Adsorption Thermodynamics and Intrinsic Activation Parameters for Monomolecular Cracking of *n*-Alkanes on Brønsted Acid Sites in Zeolites, J. Phys. Chem. C 119 (2015) 10427–10438.
[50] J.A. Swisher, N. Hansen, T. Maesen, F.J. Keil, B. Smit, A.T. Bell, Theoretical Simulation of n-Alkane Cracking on Zeolites, J. Phys. Chem. C 114 (2010) 10229–10239.
[51] A. Janda, B. Vlaisavljevich, L.-C. Lin, B. Smit, A.T. Bell, The effects of zeolite structure on adsorption thermodynamics and on apparent and intrinsic kinetics of monomolecular n-butane cracking and dehydrogenation, J. Am. Chem. Soc. 138 (2016) 4739–4756.
[52] S. Mallikarjun Sharada, P.A. Zimmerman, A.T. Bell, M. Head-Gordon, Insights into the Kinetics of Cracking and Dehydrogenation Reactions of Light Alkanes in H-MFI, J. Phys. Chem. C 117 (2013) 12600–12611.
[53] N.M. Phadke, J. Van der Mynsbrugge, E. Mansoor, A. Getsoian, M. Head-Gordon, A.T. Bell, Characterization of isolated Ga^{3+} cations in Ga/H-MFI prepared by vapor-phase exchange of H-MFI with $GaCl_3$, ACS Catal. 8 (2018) 6106–6126.
[54] J. Bandiera, Y. Ben Taârit, Ethane conversion: Kinetic evidence for the competition of consecutive steps for the same active centre, Appl. Catal. A Gen. 152 (1997) 43–51.
[55] Y. Sun, T.C. Brown, Catalytic Cracking, Dehydrogenation, and Aromatization of Isobutane over Ga/HZSM-5 and Zn/HZSM-5 at Low Pressures, Int. J. Chem. Kinet. 34 (2002) 467–480.
[56] M. Bondil, Master's Thesis, Elucidation of the catalytic properties of Ga/H-ZSM5 zeolite catalyst for light alkane dehydrogenation and dehydroaromatization chemistry, Ecole Polytechnique Fédérale de Lausanne (2017).
[57] Neelay M. Phadke, Erum Mansoor, Matthieu Bondil, Martin Head-Gordon, Alexis T. Bell, Mechanism and kinetics of propane dehydrogenation and cracking over Ga/H-MFI prepared via vapor-phase exchange of H-MFI with $GaCl_3$, J. Am. Chem. Soc. 141 (4) (2019) 1614–1627.
[58] Neelay M. Phadke, Erum Mansoor, Martin Head-Gordon, Alexis T. Bell, Mechanism and Kinetics of Light Alkane Dehydrogenation and Cracking over Isolated Ga Species in Ga/H-MFI, ACS Catal. 11 (4) (2021) 2062–2075.
[59] G. Collinge, S.F. Yuk, M.-T. Nguyen, M.-S. Lee, V.-A. Glezakou, R. Rousseau, Effect of Collective Dynamics and Anharmonicity on Entropy in Heterogenous Catalysis: Building the Case for Advanced Molecular Simulations, ACS Catal. 10 (2020) 9236–9260.
[60] J. Hajek, J. Van der Mynsbrugge, K. De Wispelaere, P. Cnudde, L. Vanduyfhuys, M. Waroquier, V. Van Speybroeck, J. Catal. 340 (2016) 227–235.
[61] P. Cnudde, K. De Wispelaere, J. Van der Mynsbrugge, M. Waroquier, V. Van Speybroeck, Effect of temperature and branching on the nature and stability of alkene cracking intermediates in H-ZSM-5, J. Catal. 345 (2017) 53–69.
[62] Paul M. Zimmerman, Diana C. Tranca, Joseph Gomes, Daniel S. Lambrecht, Martin Head-Gordon, Alexis T. Bell, Ab Initio Simulations Reveal that Reaction Dynamics Strongly Affect Product Selectivity for the Cracking of Alkanes over H-MFI, J. Am. Chem. Soc. 134 (47) (2012) 19468–19476.
[63] J. VandeVondele, M. Krack, F. Mohamed, M. Parrinello, T. Chassaing, J. Hutter, Quickstep: Fast and accurate density functional calculations using a mixed Gaussian and plane waves approach, Comput. Phys. Commun. 167 (2005) 103–128.
[64] L. Benco, T. Bucko, J. Hafner, Dehydrogenation of propane over Zn-MOR. Static and dynamic reaction energy diagram, J. Catal. 277 (1) (2011) 104–116.
[65] Tomáš Bučko, Jürgen Hafner, The role of spatial constraints and entropy in the adsorption and transformation of hydrocarbons catalyzed by zeolites, J. Catal. 329 (2015) 32–48.
[66] S.L.C. Moors, K. De Wispelaere, J. Van der Mynsbrugge, M. Waroquier, V. Van Speybroeck, ACS Catal 3 (2013) 2556–2567.
[67] J. Van der Mynsbrugge, S.L.C. Moors, K. De Wispelaere, V. Van Speybroeck, ChemCatChem 6 (2014) 1906–1918.
[68] P. Cnudde, K. De Wispelaere, J. Van der Mynsbrugge, M. Waroquier, V. Van Speybroeck, J. Catal. 345 (2017) 53–69.
[69] V. Van Speybroeck, K. De Wispelaere, J. Van der Mynsbrugge, M. Vandichel, K. Hemelsoet, M. Waroquier, First principle chemical kinetics in zeolites: the methanol-to-olefin process as a case study, Chem. Soc. Rev. 43 (2014) 7326–7357.
[70] Veronique Van Speybroeck, Karen Hemelsoet, Lennart Joos, Michel Waroquier, Robert G. Bell, C. Richard A. Catlow, Advances in theory and their application within the field of zeolite chemistry, Chem. Soc. Rev. 44 (20) (2015) 7044–7111.
[71] A. Laio, M. Parrinello, Escaping free-energy minima, Proc. Natl. Acad. Sci. 99 (20) (2002) 12562–12566.
[72] P. Fleurat-Lessard, T. Ziegler, Tracing the minimum-energy path on the free-energy surface, J. Chem. Phys. 123 (2005) 084101.
[73] Ludovico Sutto, Simone Marsili, Francesco Luigi Gervasio, New advances in metadynamics, Wiley Interdiscip, Rev.: Comput. Mol. Sci. 2 (5) (2012) 771–779.
[74] P. Bash, U. Singh, R Langridge, P. Kollman, Free energy calculations by computer simulation, Science 236 (4801) (1987) 564–568.
[75] Eric Darve, Andrew Pohorille, Calculating free energies using average force, J. Chem. Phys. 115 (20) (2001) 9169–9183.
[76] C. Jarzynski, Nonequilibrium Equality for Free Energy Differences, Phys. Rev. Lett. 78 (14) (1997) 2690–2693.
[77] E. Grifoni, G.M. Piccini, M. Parinello, Microscopic description of acid-base equilibrium, Proc. Nat. Acad. Sci. 116 (2019) 4054–4057.
[78] B. Peters, Recent advances in transition path sampling: accurate reaction coordinates, likelihood maximization and diffusive barrier-crossing dynamics, Molec. Simul. 36 (2010) 1265–1281.
[79] T. Bučko, L. Benco, O. Dubay, C. Dellago, J. Hafner, Mechanism of alkane dehydrogenation catalyzed by acidic zeolites: Ab initio transition path sampling, J. Chem. Phys. 131 (2009) 214508.
[80] Hanjun Fang, Hakan Demir, Preeti Kamakoti, David S. Sholl, Recent developments in first-principles force fields for molecules in nanoporous materials, J Mater Chem A. 2 (2) (2014) 274–291.
[81] John M. Findley, Salah Eddine Boulfelfel, Hanjun Fang, Giovanni Muraro, Peter I. Ravikovitch, David S. Sholl, A Transferable Force Field for Predicting Adsorption and Diffusion of Hydrocarbons and Small Molecules in Silica Zeolites with Coupled-Cluster Accuracy, J Phys Chem C. 125 (15) (2021) 8418–8429.